Earth-Science Reviews 212 (2021) 103448

Contents lists available at ScienceDirect

Earth-Science Reviews

journal homepage: www.elsevier.com/locate/earscirev

Magmatic responses to Cretaceous subduction and tearing of the paleo-Pacific Plate in SE China: An overview

Feng Guo [a,b,*], Yangming Wu [c], Bo Zhang [a], Xiaobing Zhang [a,d], Liang Zhao [a,b], Jie Liao [c]

[a] State Key Laboratory of Isotope Geochemistry, Guangzhou Institute of Geochemistry, Chinese Academy of Sciences, Guangzhou 510640, China
[b] Innovation Academy for Earth Science, CAS, Beijing 100029, China
[c] School of Earth Sciences and Engineering, Sun Yat-Sen University, Guangzhou 510275, China
[d] College of Earth and Planetary Sciences, University of Chinese Academy of Sciences, Beijing 100049, China

ARTICLE INFO

Keywords:
Arc-type mafic rocks
Intraplate basalts
Paleo-Pacific subduction
Slab tearing
Cretaceous
SE China

ABSTRACT

Both Cretaceous arc-type and intraplate rocks are widely distributed in SE China, in association with subduction of the paleo-Pacific Plate. However, it remains unclear whether there exists a genetic link between the intraplate and subduction-related magmatism. Here we conduct a comprehensive geochemical data compilation, sorting and processing of the Cretaceous mafic igneous rocks from SE China, in combination with a 2-D numerical simulation on slab melting, to further decipher the petrogenetic relationship between the arc-type and intraplate magmatism under a unified tectonic framework invoking subduction and rollback-tearing of the paleo-Pacific Ocean.

The Cretaceous arc-type mafic rocks (120–80 Ma) include eruptive and intrusive rocks, distributing along the coastal region in a NE-NNE direction. After parent magma compositional recalculation of the mafic intrusions, the results indicate that both the eruptive and intrusive arc-type mafic rocks are hydrous calc-alkaline basalts, with enrichments in large ion lithophile elements (LILEs) and light rare earth elements (LREEs) but depletions in high field strength elements (HFSEs), crust-like Sr-Nd-Pb-Hf isotopic compositions, and low Lu/Hf ratios. All these features are typical of igneous rocks formed in a continental arc. The combined data suggest their mantle source was mainly metasomatized by melts derived from the subducted terrestrial sediments and reflect a relatively hot subduction zone during Cretaceous.

The intraplate mafic rocks (110–70 Ma) distribute in SE China interior and generally show trace element geochemistry similar to oceanic island basalt (OIB, hereafter we term them as OIB-like basalts). They can be further divided into two groups: high-Nb (Nb > 50 ppm) and low-Nb (Nb < 40 ppm) basalts. The high-Nb basalts have depleted asthenospheric mantle-like isotopic compositions. Their mantle source was composed mainly of pyroxenite that was likely formed through interaction between the asthenosphere and melts from the dehydrated subducted slab. Relative to the high-Nb basalts, the low-Nb basalts have lower Nb/REE and Nb/LILE ratios, and more evolved but highly variable isotopic compositions. Their mantle source was also the asthenosphere metasomatized by addition of the slab melts containing a higher proportion of recycled sediment component.

From the arc-type to low-Nb and ultimately to high-Nb mafic rocks, increases of Nb, Nb/LILE and Nb/REE ratios are coupled with more depleted Sr-Nd-Pb-Hf isotopic features, reflecting the occurrence of melting from the upper subducted sediment to the lower oceanic mafic crust that had experienced extensive dehydration. Further thermodynamic modelling results show that melting of the dehydrated slab can occur along the torn surface and lower part of the oceanic crust, once the slab is strongly thinned and fractured in response to tearing and fragmentation. In combination with the contemporaneous sedimentary records in SE China, the Cretaceous mafic magmatism provided geochemical records of tectonic transition from early Cretaceous advanced subduction to late Cretaceous rollback of the paleo-Pacific slab, during which slab tearing or fragmentation and the resultant melting of the dehydrated subducted slab acted as a predominant agent for mantle enrichment.

* Corresponding author at: State Key Laboratory of Isotope Geochemistry, Guangzhou Institute of Geochemistry, Chinese Academy of Sciences, Guangzhou 510640, China.
E-mail address: guofengt@263.net (F. Guo).

https://doi.org/10.1016/j.earscirev.2020.103448
Received 14 June 2020; Received in revised form 15 November 2020; Accepted 17 November 2020
Available online 25 November 2020

1. Introduction

Subduction zone is a major site for mass and energy exchange between the crust and mantle, and a crucial place of continental crust growth, accretion and modification. It is also the most important zone of earthquake, lithospheric deformation, magmatism and mineralization (e.g., Stern, 2002). The total length of present subduction zone on the Earth is more than 40,000 km, with 2.5–3.0 km^3 of sediments are recycled into the mantle every year (von Huene and Scholl, 1991; Clift et al., 2009; Scholl and Von Huene, 2010), which causes wide compositional and isotopic ranges for the subduction-related and oceanic island basalts (e.g., Weaver, 1991; Hoffman, 1997; Plank and Langmuir, 1998). Although numerous studies have been focused on the subduction of oceanic and continental lithosphere, the key issues such as the mechanism of subduction initiation, the metasomatism operating in the mantle wedge and the fate of the subducted slab (e.g., Stern, 2004; Spandler and Pirard, 2013; Gréaux et al., 2019), remain highly controversial. Answers to these questions will not only deepen our understanding on the mass and energy cycling in the deep Earth but also facilitate the development of plate tectonics.

At subduction zones, the magmatism is characterized by emplacement of voluminous andesites and mafic magmas (e.g., Grove and Kinzler, 1986; Kelemen et al., 2013; Stern, 2002). The mafic magmas consist mainly of hydrous tholeiitic to calc-alkaline basalts, which are characterized by enrichments in LILEs and LREEs relative to HFSEs, such as Nb and Ta (e.g., Stolz et al., 1996; Plank et al., 2013). The LILE enrichment has been widely considered as a result of preferential mobilization of LILEs in fluids from the slab to mantle wedge (e.g., Spandler and Pirard, 2013). In contrast, the HFSE depletion has been largely ascribed to the lower solubility of HFSEs in slab-derived fluids and/or melts as the HFSE-rich minerals are retained in the residual downgoing slab (Klemme et al., 2005 and references therein). However, the arc basalts have been partially or even completely unroofed and eroded in many paleo-subduction zones, such as in SE China and NE China (e.g., Guo et al., 2016; Zhang et al., 2019; Zhao et al., 2019). The subduction-related mafic intrusions, which usually occur as mafic cumulates, may provide geochemical information about the evolution of the paleo-subduction zones once the composition of their parental magmas can be recalculated (e.g., Guo et al., 2015, 2016).

Apart from the arc magmas, there also exist some mafic magmas with geochemical features similar to oceanic island basalts (OIBs, having negligible HFSE depletion or even Nb and Ta enrichment in primitive mantle (PM)-normalized spidergrams) at subduction zones, e.g., Cascades (Mullen and Weis, 2013), Mexico (Castillo, 2008; Gómez-Tuena et al., 2018a and references therein), Nicaragua (Gazel et al., 2011), Costa Rica (e.g., Reagan and Gill, 1989), eastern Jamaica (Hastie et al., 2011), southern Patagonian (e.g., Espinoza et al., 2005), Kamchatka (Kepezhinskas et al., 1997 and references therein), SE China (Cui et al., 2011; Zhang et al., 2020) and southern Philippines (Castillo, 2008). The origin of such OIB-like magmatism remains highly debatable. Petrogenetic models, such as (1) presence of mantle plume or plume-slab interaction (Gazel et al., 2011; Márquez et al., 1999 and references therein); (2) asthenospheric upwelling via slab window (Espinoza et al., 2005; Mullen and Weis, 2013 and references therein); (3) asthenospheric diapir (e.g., Ferrari, 2004); (4) incorporation of exotic enriched mantle via corner flow into mantle wedge (Ferrari et al., 2001; Herrstrom et al., 1995); and (5) slab melt-metasomatized mantle wedge above a subduction zone (e.g., Kepezhinskas et al., 1997), have been proposed. Theoretically, the OIB-like geochemistry in such igneous rocks requires involvement of enriched components in the source, e.g., either derivation from a recent subducted slab or inheritance from an OIB-type mantle domain and/or both (Gazel et al., 2011; Gorring et al., 2003; Hastie et al., 2011; Zhang et al., 2020). Identification of the recycled enriched components is therefore crucial in understanding the mantle geodynamics and mass recycling in the deep Earth.

SE China has been an active continental margin that was formed by subduction of the paleo-Pacific Ocean beneath the Eurasian continent during Mesozoic time (e.g., Liu et al., 2012; Liu et al., 2016b; Zeng et al., 2016; Zhao et al., 2016; Zhou and Li, 2000). Besides the Cretaceous subduction-related magmatism (e.g., arc-type basalts and mafic intrusions between 120 and 77 Ma) in the region (Zhang et al., 2019 and references therein), there also distributes OIB-like magmatism of 110–70 Ma (Wang et al., 2003, 2008, 2013; Cui et al., 2011; Zhang et al., 2020; Wu et al., 2020). However, it remains controversial about the genetic relationship between the intraplate and subduction-related magmatism. In this contribution, we carry out a comprehensive compilation, sorting and processing of the geochemical data of the Cretaceous arc-type and OIB-like mafic igneous rocks in SE China, and perform a two-dimensional numerical simulation of melting of a dehydrated slab. Based on a new classification scheme of the OIB-like rocks and parental magma recalculation of the mafic intrusions, we discover systematic geochemical variations from the arc-type to low-Nb and ultimately to high-Nb rocks, reflecting the involvement of enriched component varying from the subducted sediment to the dehydrated oceanic mafic crust in the mantle source. This transition of mantle metasomatism was consistent with the subduction and rollback of the subducting paleo-Pacific oceanic slab from early to late Cretaceous. Further numerical modelling results suggest the melting of dehydrated oceanic crust only in a strongly thinned slab, probably as a consequence of tearing and fragmentation of the subducted slab. Integrating with the regional sedimentary records, we propose that the tectonic transition from early Cretaceous advanced subduction to late Cretaceous rollback-tearing of the paleo-Pacific slab was response for the emplacement of both the arc-type and OIB-like mafic magmatism in SE China.

2. Geological Backgrounds

The South China Block is separated from the North China Craton by the Qinling-Dabie orogen, and consists of the Cathaysia Block in the southeast and the Yangtze Block in the northwest (Fig. 1). These two blocks have different Precambrian basements. The Yangtze basement rocks consist predominantly of Archean (ca. 3.8–2.9 Ga) tonalite, trondhjemite, and granodiorite gneisses and metasedimentary rocks in the Kongling Complex (Gao et al., 2011). The basement rocks of the Cathaysia Block are mainly composed of Paleoproterozoic to Neoproterozoic gneiss, amphibolite, migmatite, and meta-volcanic rocks (Yu et al., 2007). The amalgamation between the Yangtze and Cathaysian blocks probably occurred during the Neoproterozoic (ca. 1.0–0.8 Ga) (e.g., Li et al., 2009).

The Mesozoic geology of SE China is characterized by emplacement of voluminous magmas with compositional variations from mafic to felsic, which has been widely considered to result from subduction of the paleo-Pacific Ocean (e.g., Lapierre et al., 1997; Zhou et al., 2006; Li and Li, 2007; Wang et al., 2016; Li et al., 2019). The Jurassic-early Cretaceous tectonic-magmatic evolution began with a crustal contraction event that gave rise to regional-scale NE-trending folds, overthrust nappes, and crustal anataxis (e.g., Wang et al., 2013; Li et al., 2019). The subsequent crustal extension produced voluminous A- and I-type granites and bimodal magmatism, accompanied with doming structures and extensional basins (e.g., Li, 2000; Li et al., 2014a, 2014b).

A remarkable feature of SE China is the presence of a Mesozoic large igneous province, which covers an area of 800 × 1400 km^2 (Fig. 1). It consists predominantly (> 90% in volume) of felsic igneous rocks and subordinately of mafic intrusive and eruptive rocks (< 10%) (Zhou and Li, 2000; Guo et al., 2012). The youthening of felsic magmatism from the continental interior to the coastal region of SE China, an abrupt increase of magma temperature and the compositional change from calc-alkaline I-type to A-type granitoids during Cretaceous (e.g., Chen and Jahn, 1998; Chen et al., 2000; Guo et al., 2012; Li et al., 2014b; Li et al., 2019), suggest rollback of the subducted paleo-Pacific Plate and the resultant asthenospheric upwelling.

Along the coastal region of SE China distribute the early Cretaceous

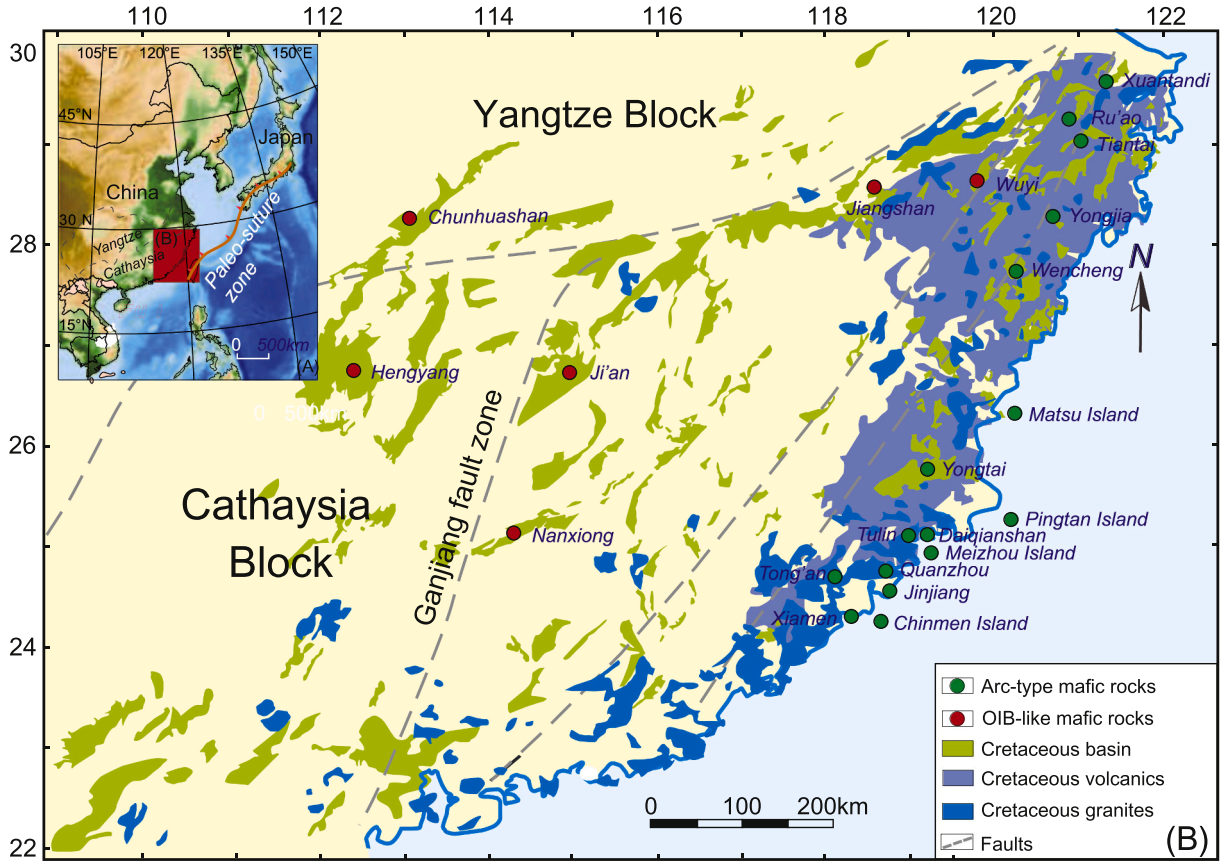

Fig. 1. A simplified tectonic map showing the distribution of Cretaceous mafic magmatism in SE China (modified after Wu et al., 2020).

calc-alkaline basalts and mafic intrusions with significant Nb—Ta negative anomalies (e.g., Nb/La < 0.6) in PM-normalized trace element spidergrams. These mafic rocks have been widely interpreted as arc-type magmas related to subduction of the paleo-Pacific Plate (e.g., Lapierre et al., 1997; Xu et al., 1999; Li et al., 2014b; Zhang et al., 2019). In contrast, some alkaline mafic lavas (110–70 Ma) were erupted or intruded in SE China with OIB-like geochemistry (e.g., Nb/La > 0.9) and have been ever regarded as continental intraplate basalts (Wang et al., 2003, 2008; Shu et al., 2004; Chen et al., 2005, 2008; Meng et al., 2012). Such spatial and temporal geochemical variations in mafic magmatism were likely a consequence of retreat of the trench and rollback of the subducting paleo-Pacific oceanic plate since Cretaceous (Liu et al., 2012; Meng et al., 2012; Li et al., 2014b; Wang et al., 2016).

From north to south, the locations of Cretaceous arc-type mafic rocks include Xuantandi, Ru'ao, Tiantai, Yongjia, Wencheng, Matsu, Yongtai, Pingtan, Daiqianshan, Meizhou, Quanzhou, Tong'an and Chinmen (e.g., Dong et al., 1997, 2007; Xu et al., 1999; Yang et al., 1999; Xie et al., 2001; Zhao et al., 2007; Cui et al., 2011). The rock types include basalt, basaltic andesite, hornblende gabbro and mafic dykes. Most of the gabbroic intrusions (e.g., Pingtan, Daiqianshan and Quanzhou) are mafic cumulates with variable degrees of plagioclase and hornblende accumulation (Dong et al., 1997; Xu et al., 1999; Zhang et al., 2019).

The Cretaceous OIB-like mafic rocks are usually distributed in SE China interior with the exception of Wuyi basin, in which both dolerite sill and basalt occur. The other locations, from north to south, include Jiangshan, Chunhuashan, Ji'an, Hengyang and Nanxiong (e.g., Li, 2000; Wang et al., 2003, 2008; Shu et al., 2004; Meng et al., 2012; Qin et al., 2019; Table S1). These basalts occur in the Cretaceous rift basins, as either interbeds or sills within the red beds.

3. Data selection, sorting and processing

Regardless of a large dataset of the Cretaceous mafic rocks in SE China, we only consider mafic rocks with SiO_2 < 54 wt% and MgO > 4 wt% with loss of ignition less than 4.5 wt% for most samples during the data selection and sorting (Table S1). Only two high-Nb basalt samples from the Liuyang basin, which have the highest $\varepsilon_{Nd}(t)$ values up to 7.6–8.0 and LOI > 5.0 wt%, are selected for constraining the endmember components. In SE China interior, such as in Huichang, Guangfeng and Shangrao basins (Liao et al., 1999; Yu et al., 2004; Chen et al., 2008; Xie et al., 2006), we preclude the samples of lamprophyre and shoshonitic basalts, which show significant Nb—Ta depletion in PM-normalized spidergrams and highly enriched Sr-Nd-Pb isotopic signatures. The reasons include: (1) Although these rocks show arc-like trace element features (obvious Nb—Ta depletions), they occur far (>400 km) away from the paleo-Pacific subduction zone and cannot represent the subduction-related magmas; (2) their highly enriched Sr-Nd-Pb isotopic signatures have been ever interpreted as low-degree melts of an old enriched lithospheric mantle of the Cathaysia Block (Chen et al., 2005; Xie et al., 2006); and (3) they are geochemically distinct from OIB-like intraplate basalts with an insignificant contribution of the subducted slab component.

We divided the arc-type mafic rocks in SE China into eruptive and intrusive types. Since the mafic dykes generally show no tracer of accumulation with similar texture to the basaltic lavas (e.g., Xie et al., 2006; Qin et al., 2010; Li et al., 2018), they are also classified as eruptive rocks without further parental magma compositional calculation. The mafic intrusions in SE China show variable effects of crystal accumulation (plagioclase and hornblende), so the whole-rock geochemistry cannot represent the parental magma composition; instead, it reflects the sum of composition of the accumulative crystals and trapped melts

(Bédard, 1994; Guo et al., 2015). During the data processing, we recalculated the parental magma compositions of these mafic intrusions by using the equilibrium distribution method reported in Guo et al. (2016) and listed the results in Table S2. The detailed description of the method is summarized below.

Mass-balance equation (Eq. (1)) expresses the concentration of an element 'i' in the cumulate rock as the sum of the products of the modal proportions φ (weight equivalents as fractions the concentrations (C) of element 'i' in the constituent minerals and the trapped melt (TM). In the Cretaceous mafic intrusions in SE China, the main crystallizing phase include hornblende, plagioclase, clinopyroxene (minor) and accessories are apatite, ilmenite, magnetite and zircon. Therefore, the trace element concentration of the diorites can be expressed as:

$C^{rock}_i = \varphi^{Hb}C^{Hb}_i + \varphi^{Cpx}C^{Cpx}_i + \varphi^{Pl}C^{Pl}_i + \varphi^{Mt}C^{Mt}_i + \varphi^{Ap}C^{Ap}_i + \varphi^{Ilm}C^{Ilm}_i +/- \varphi^{Zr}C^{Zr}_i + \varphi^{TM}C^{TM}_i$ (1).

By definition:

$C^{Hb}_i = C^{Pl}_i({}^{Hb/melt}D_i/{}^{Pl/melt}D_i) = C^{Cpx}_i({}^{Hb/melt}D_i/{}^{Cpx/melt}D_i) = C^{Ilm}_i({}^{Hb/melt}D_i/{}^{Ilm/melt}D_i) = C^{Mt}_i ({}^{Hb/melt}D_i/{}^{Mt/melt}D_i) = C^{Ap}_i({}^{Hb/melt}D_i/{}^{Ap/melt}D_i) = C^{Zr}_i({}^{Hb/melt}D_i/{}^{Zr/melt}D_i)$ (2).

The equilibrium distribution of trace elements among the constituent minerals can be calculated when Eq. (2) is substituted into Eq. (1). Setting the crystal/liquid partition coefficient (D) for the trapped melt at 1.0, then the equation has this form for the hornblende solution, with φ^{TM} as the only unknown:

$C^{Hb}_i = C^{rock}_i/\{\varphi^{Hb} + (\varphi^{CpxCpx/melt}D_i/{}^{Hb/melt}D_i) + (\varphi^{PlPl/melt}D_i/{}^{Hb/melt}D_i) + (\varphi^{MtMt/melt}D_i/{}^{Hb/melt}D_i) + (\varphi^{IlmIlm/melt}D_i/{}^{Cpx/melt}D_i + (\varphi^{ApAp/melt}D_i/{}^{Hb/melt}D_i) +/- (\varphi^{ZrZr/melt}D_i/{}^{Hb/melt}D_i) + ((\varphi^{TM}{}^{Cpx/melt}D_i)\}$ (3).

This eq. (3) yields the hornblende trace element concentration, and division by the partition coefficient ($^{Hb/melt}D$), gives the concentration of the element in the coexisting equilibrium liquid ($C^{melt}_i = C^{Hb}_i/{}^{Hb/melt}D_i$).

To simplify the calculation, the hornblende gabbro intrusion is also reduced to two- or three-phase assemblage with 15–20% trapped melt by using a non-modal melting backstripping procedure. In the following text and related figures, we will therefore use the recalculated results instead of the measured values, especially the trace element concentrations of the mafic intrusions.

Although there distribute many Cretaceous basaltic/mafic rocks in the continental interior of SE China, we only select the OIB-like samples with Nb/La > 0.9. There are some mafic sills with OIB-like geochemistry (the dolerite sill in Wuyi basin), these rocks show no tracer of crystal accumulation and are also regarded as eruptive basalts (Zhang et al., 2020).

The primitive magma composition of basalts can be calculated through addition of olivine back into the melt until chemical equilibrium between the estimated primitive magma and mantle olivine is reached (Wang et al., 2012). In this paper, we only select the high-Nb basalt samples that have experienced olivine-dominated fractionation with negligible crustal contamination through addition of olivine in 0.1% increments (assuming that 10% of the total iron is Fe^{3+} and $(Fe^{2+}/Mg)_{olivine}/(Fe^{2+}/Mg)_{melt} = 0.3$). The compositions of primitive melts are then obtained through addition of olivine in 0.1% increments until the equilibrium between the melt and olivine of maximum Fo_{90} is reached.

4. Geochemistry of the Cretaceous mafic igneous rocks

The Cretaceous mafic rocks in SE China span a large range of SiO_2 from 38.1 to 53.6 wt%, a range of $Na_2O + K_2O$ from 1.2 to 7.2 wt%, a MgO range between 4.0 and 10 wt% with a Mg# (Mg# = 100 Mg/(Mg + ∑Fe) in atomic ratio) range from 41.5 to 68.1. Another remarkable feature is the wide Nb range from 1.0 to 87.1 ppm. To better describe these mafic rocks, we divide the OIB-like rocks into two groups: high-Nb basalt with Nb > 50 ppm (51.4–87.1 ppm) and Nb/Y > 2.0 and low-Nb basalt with Nb < 40 ppm (14.4–37.7 ppm) and Nb/Y < 2.0. The arc mafic intrusions generally have lower contents of SiO_2 and $Na_2O + K_2O$ and show a positive correlation between them (Fig. S1a), as a result of plagioclase and hornblende accumulation (Dong et al., 1997; Xu et al., 1999; Zhang et al., 2019). The high-Nb basalts have the highest $Na_2O + K_2O$, while the arc-type basaltic lavas and low-Nb basalts have comparative contents of SiO_2 and $Na_2O + K_2O$. However, the correlations between SiO_2 and Mg# are lacking in all three rock types (Fig. S1b). After mass balance calculation on the arc mafic intrusions, the Cretaceous mafic rocks in SE China include a variety of rock types from subalkaline basalt and basaltic andesite, alkaline basalt to strongly alkaline basalt in a Nb/Y versus $10^{-4} \times Zr/TiO_2$ plot (Fig. 2a). From the high-Nb to low-Nb and then to arc-type mafic rocks, the decrease of Nb is coupled with a decrease of Nb/U and increases of Ba/Nb and Zr/Nb (Fig. 2b-d).

4.1. Geochemistry of the Cretaceous arc-type mafic magmatism

The Cretaceous arc-type mafic rocks consist of sub-alkaline basalts and basaltic andesites and their intrusive counterparts. Compared with the OIB-like rocks in SE China interior, the arc-type mafic rocks have much lower Nb (1.0–14.6 ppm) concentrations and thus show lower Nb/Y, Nb/U and higher Ba/Nb, Zr/Nb, La/Nb and Th/Nb ratios (Fig. 2 and Table S1).

The arc-type basaltic lavas are characterized by right-declined chondrite-normalized REE patterns with LREE enrichment relative to HREE and some samples have positive Eu anomalies (Fig. 3a). The mafic intrusions (mainly hornblende gabbros) show variable enrichment in LREEs and depletions in HREE with variable Eu anomalies. Some samples display convex REE patterns with middle REE (e.g., Nd) enrichment that is typical of hornblende accumulation (Fig. 3b). After the mass balance calculation, all arc-type mafic rocks show Nb—Ta depletions and LILE and LREE enrichments in the PM-normalized spidergrams (Fig. 4a and b). They are geochemically distinct from the OIB-like rocks and plot within the fields of arc volcanics in La/Nb versus Ba/Nb and triangle diagrams of La-Nb-Y and Th-Ta-Hf (Fig. 5a, c and d), and from a hydrate mantle source in a $(Ta/La)_{PM}$ versus $(Hf/Sm)_{PM}$ plot (Fig. 5b).

The Cretaceous arc-type mafic rocks generally show crust-like isotopic signatures, with negative $\varepsilon_{Nd}(t)$ values from −4.7 to −0.2. They also have moderately radiogenic Sr with an $^{87}Sr/^{86}Sr(i)$ range from 0.70478 to 0.70732, and radiogenic Pb compositions, with a $^{206}Pb/^{204}Pb(i)$ range from 18.13 to 18.60, and a $^{207}Pb/^{204}Pb(i)$ range from 15.57 to 15.66 and a $^{208}Pb/^{204}Pb(i)$ range from 38.19 to 38.79 (Table S1 and Fig. 6). Available whole-rock Hf isotope compositions from the Pingtan, Daiqianshan and Quanzhou mafic intrusions show that they have weakly positive $\varepsilon_{Hf}(t)$ values from +0.5 to +3.9 (Zhang et al., 2019). The arc-type mafic rocks in SE China have Sr-Nd-Pb-Hf isotopic compositions similar to those arc magmas from SW Japan (Fig. 6, Ishizaka and Carlson, 1983; Shimoda et al., 1998; Tatsumi et al., 2003), which have been interpreted as melts from a mantle wedge metasomatized by recycled sediments.

4.2. Geochemistry of the Cretaceous OIB-like basalts

The Cretaceous OIB-like basalts in SE China occur as basaltic lavas and mafic sills. According to previous studies (e.g., Wang et al., 2003, 2008; Cui et al., 2011; Meng et al., 2012; Shu et al., 2015; Qin et al., 2019; Wu et al., 2020), both high-Nb and low-Nb basalts occur in the Ji'an (Luosishan) and Liuyang (Chunhuashan) basins, whereas only low-Nb basalts occur in the other localities such as in the Wuyi and Jiangshan basins in Zhejiang province, Hengyang basin in Hunan province and Nanxiong basin in Guangdong province (Table S1). In general, the high-Nb basalts have lower SiO_2, higher P_2O_5, TiO_2 and K_2O contents than the low-Nb basalts (Table S1 and Fig. S1a).

All OIB-like basalts show steeply right-declined REE patterns, with enrichment in LREEs and depletion in HREEs and an insignificant Eu anomaly (Fig. 3c and d). However, the high-Nb basalts generally have higher LREE concentrations than but similar HREE contents to the low-Nb basalts (Fig. 3d). In the PM-normalized incompatible element

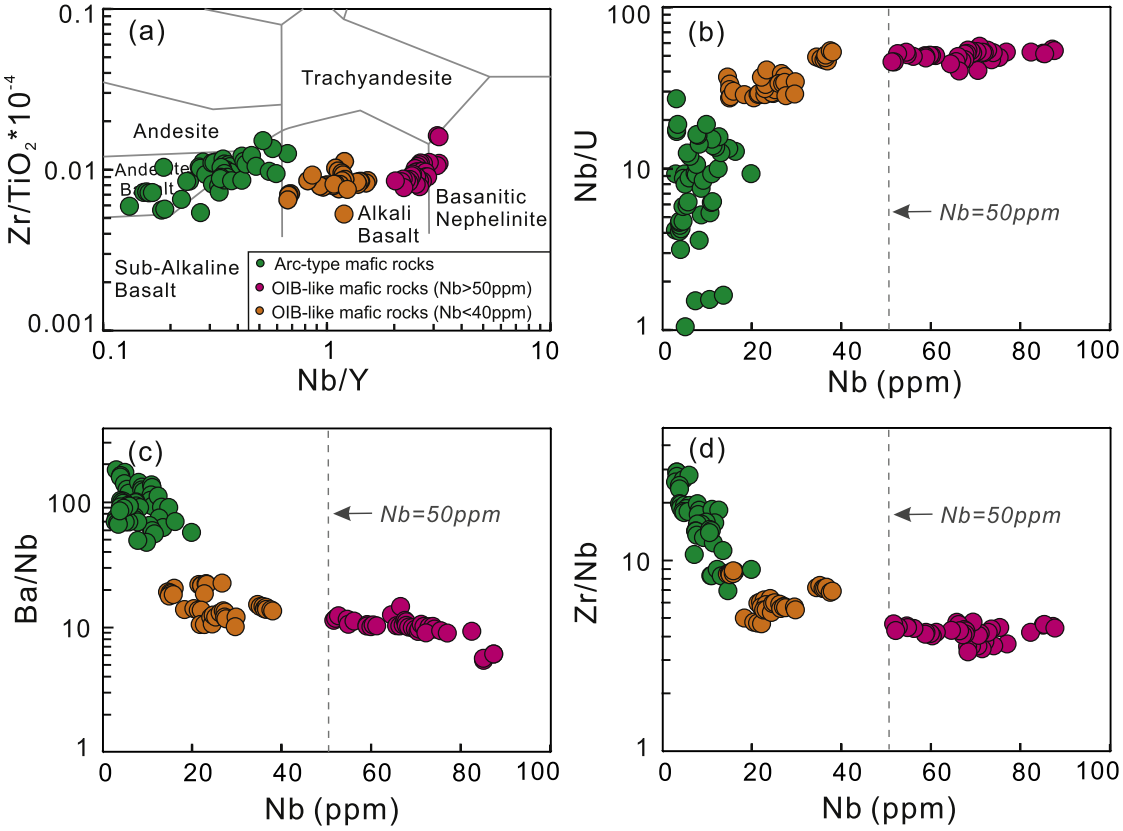

Fig. 2. Nb/Y versus 10^{-4} × Zr/TiO_2 (a, Winchester and Floyd, 1977), Nb versus Nb/U (b), Ba/Nb (c) and Zr/Nb (d) plots, showing a new classification scheme of Cretaceous mafic rocks in SE China. Data sources are from Supplementary Table 1 (Table 1S).

spidergrams, the high-Nb basalts are characterized by positive Nb—Ta anomalies and a prominent negative Pb anomaly (Fig. 4c). Also, most samples show Sr—Ba enrichments. By contrast, the low-Nb basalts show insignificant Nb—Ta enrichment but with large fluctuations in most incompatible elements such as Rb, K and Pb (Fig. 4d). In addition, the Cretaceous OIB-like basalts have similar La/Nb, Ba/Nb, $(Ta/La)_{PM}$ and $(Hf/Sm)_{PM}$ ratios to the counterparts occurring in oceanic islands (Fig. 5a and b). In the triangle diagrams of La-Nb-Y and Th-Ta-Hf (Fig. 5c and d), they are again plotted within the fields defined by continental rift or intraplate basalts (Li et al., 2015).

Although both groups show OIB-like trace element geochemistry, the high-Nb basalts generally have higher Nd and Hf and low Sr isotope compositions than the low-Nb basalts (Table 1). For instance, the high-Nb basalts generally have a range of $^{87}Sr/^{86}Sr(i)$ between 0.70323 and 0.70455 and an $\varepsilon_{Nd}(t)$ range from +5.0 to +8.0. The high-Nb basalts from the Chunhuashan area have the highest $\varepsilon_{Nd}(t)$ as high as +8.0 and the lowest $^{87}Sr/^{86}Sr(i)$ to 0.7032 (Wang et al., 2008), whereas the low-Nb basalts from the Hengyang basin have the lowest $\varepsilon_{Nd}(t)$ value as low as −1.7 and the highest $^{87}Sr/^{86}Sr(i)$ up to 0.7075 (Meng et al., 2012). A few whole-rock Hf isotopic compositions from both the high-Nb and low-Nb basalts show positive $\varepsilon_{Hf}(t)$ values from +4.2 to +9.7 (Wu et al., 2020; Zhang et al., 2020). Also, the high-Nb basalts in the Ji'an basin show moderately radiogenic Os ($^{187}Os/^{186}Os(i)$ = 0.1676–0.2076, Wu et al., 2020), and the low-Nb basalts in the Wuyi basin show light Ca isotopic compositions ($\delta^{44}/^{40}Ca$ = 0.65–0.72‰, Zhang et al., 2020). The high-Nb basalts show narrow variation in Pb isotope compositions, for instance, they span a $^{206}Pb/^{204}Pb(i)$ range from 18.36 to 18.48, and a $^{207}Pb/^{204}Pb(i)$ range from 15.55 to 15.60 and a $^{208}Pb/^{204}Pb(i)$ range from 38.43 to 38.59 (Table S1 and Fig. 6). In contrast, the low-Nb basalts show large variations in Pb isotope data, spanning a $^{206}Pb/^{204}Pb(i)$ range from 18.18 to 18.63, and a $^{207}Pb/^{204}Pb(i)$ range from 15.57 to 15.62 and a $^{208}Pb/^{204}Pb(i)$ range from 38.58 to 38.88 (Table S1 and Fig. 6).

5. Origin of Cretaceous mafic igneous rocks in SE China

The Cretaceous mafic igneous rocks in SE China show large geochemical variations from sub-alkaline to strongly alkaline affinities, a range of Nb from 1.0 ppm to 87 ppm and an $\varepsilon_{Nd}(t)$ range from −4.7 to +8.0. From the arc-type to low-Nb and ultimately to the high-Nb mafic rocks, following the increases of Nb or Nb/Y ratio, the Sr-Nd-Hf isotopic compositions become more depleted toward the values of depleted asthenospheric mantle (Figs. 2 and 6). This suggests that the contribution of a depleted mantle (e.g., high $\varepsilon_{Nd}(t)$ and Nb/U) becomes more and more significant; whereas the contribution of crustal components (e.g., high Th/Nb and $^{87}Sr/^{86}Sr(i)$ and low Nb/U, Plank and Langmuir, 1998; Table 1) becomes less important in the petrogenesis. In the following, we will give a comprehensive review on the origins of arc-type mafic rocks and OIB-like basalts, mainly focused on the magmatic evolution and source characteristics.

5.1. Origin of arc-type mafic rocks

The arc-type mafic rocks in SE China generally show crust-like isotopic features, e.g., moderately radiogenic Sr and Pb compositions and negative $\varepsilon_{Nd}(t)$ values. Such features have been ever considered either as a result of crustal contamination during the magmatic evolution or as a consequence of source contamination through mantle-crust interaction at subduction zones (e.g., Xu et al., 1999; Dong et al., 1997; Griffin et al., 2002; Zhang et al., 2019). It is therefore essential to distinguish these two processes before the reliable petrogenetic hypothesis can be obtained.

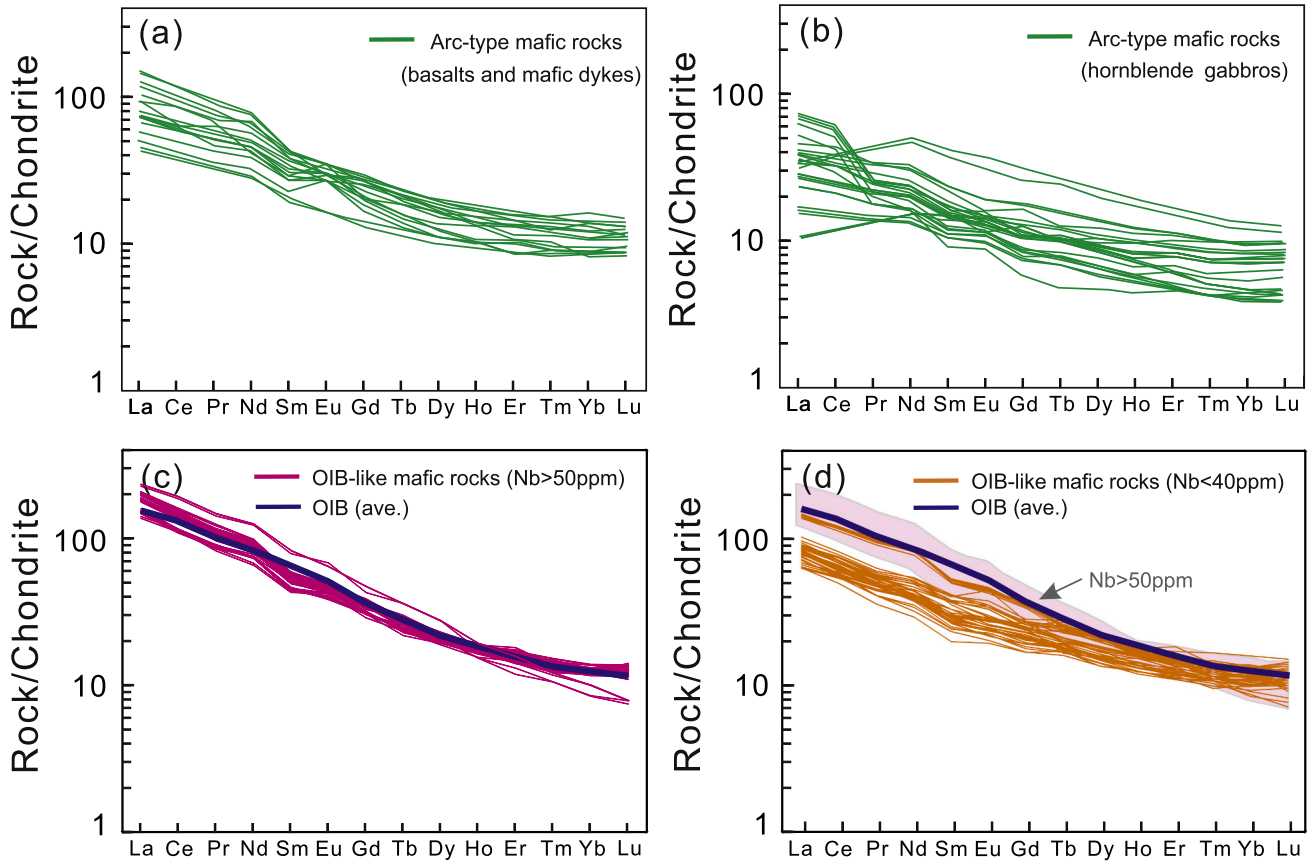

Fig. 3. Chondrite-normalized REE patterns of Cretaceous mafic rocks in SE China. Normalized values of chondrite are from Sun and McDonough (1989). Data sources are the same as Fig. 2.

5.1.1. Magmatic differentiation

In a magmatic system, close-system evolution will crystallize minerals with identical isotope composition to the parental magma, whereas the crystallizing minerals may have different isotope compositions from the primitive magma in an open-system chamber via crustal contamination or assimilation. This enables us to identify the effect of crustal contamination by comparing the isotopic compositions, which are sensitive to open-system evolution like Sr and Pb isotopes, between mineral and bulk rock. Petrographic observations indicate plagioclase an early crystallizing phase in all arc-type mafic intrusions (e.g., Dong et al., 1997; Xu et al., 1999; Zhang et al., 2019), suggesting that Sr and Pb isotope compositional comparison between plagioclase and whole rock can be applied to distinguish whether these mafic intrusions experienced an open-system magmatic evolution or not. Zhang et al. (2019) conducted in-situ isotopic analyses (Sr and Pb isotopes) on plagioclase from three mafic intrusions respectively at Pingtan, Daiqianshan and Quanzhou, yielding almost identical Sr and Pb isotope compositions between the plagioclase and whole rock in each intrusion. Their results indicate the close-system magmatic evolution with a negligible effect of crustal assimilation for the arc mafic intrusions.

Although there lack available in-situ isotope analyses on individual minerals (e.g., plagioclase and clinopyroxene) to discuss the role of crustal contamination or assimilation-fractional crystallization (AFC) processes in the formation of the arc-type basaltic lavas and mafic dykes, other geochemical index (e.g., SiO_2 and Nb/La versus Sr and Nd isotope compositions) of the mafic rocks also argue against the important effect of open-system magmatic processes (e.g., Xie et al., 2001; Qin et al., 2010, 2019; Cui et al., 2011; Li et al., 2018). In fact, most of these eruptive mafic lavas and intrusive rocks show limited Sr—Nd isotopic variations against a large range of La/Nb and Mg# (e.g., Zhang et al., 2019), precluding a significant role of crustal contamination or AFC processes during the magmatic evolution. In general, primary mantle-derived mafic melts have Ni > 400 ppm and Cr > 1000 ppm, and Mg# = 73–81 (Wilson, 1989). The arc-type mafic rocks in SE China show relatively low Mg# (41–68) and compatible element contents such as Cr (9–649 ppm) and Ni (5–217 ppm), indicating a significant fractionation of olivine, clinopyroxene and hornblende. Consequently, compared to the insignificant effect of open-system evolution, the role of close-system magmatic processes, such as fractional crystallization and crystal (plagioclase and hornblende) accumulation, is more important to interpret the wide compositional ranges of the arc-type mafic rocks in SE China (e.g., Zhang et al., 2019).

The occurrence of calcic plagioclase (An >90) and abundant hornblende indicates that the parental magmas for the hornblende gabbro at Pingtan, Daiqianshan and Quanzhou were water-saturated with H_2O more than 5% (Dong et al., 1997; Xu et al., 1999; Zhang et al., 2019). Although the water estimation of the basaltic lavas and mafic sills is yet lacking, the occurrence of hydroxyl hornblende phenocryst in these rocks likely suggests that their parental magmas were water-saturated.

In summary, the parent magmas of the arc-type mafic rocks (both intrusive and extrusive rocks) in SE China were hydrous and experienced close-system magmatic evolution such as fractionation or accumulation with an insignificant effect of crustal assimilation.

5.1.2. Nature of mantle source

Since the role of crustal contamination or assimilation is negligible and the fractionation and/or accumulation of mafic minerals and plagioclase has little influence on the LILE/HFSE and LREE/HFSE ratios and isotopic compositions, such crust-like geochemical features in the arc-type mafic rocks in SE China are probably resulted from source enrichment via subduction, as indicated from the tectonic reconstruction of the paleo-Pacific Plate (e.g., Sun et al., 2007; Seton et al., 2012).

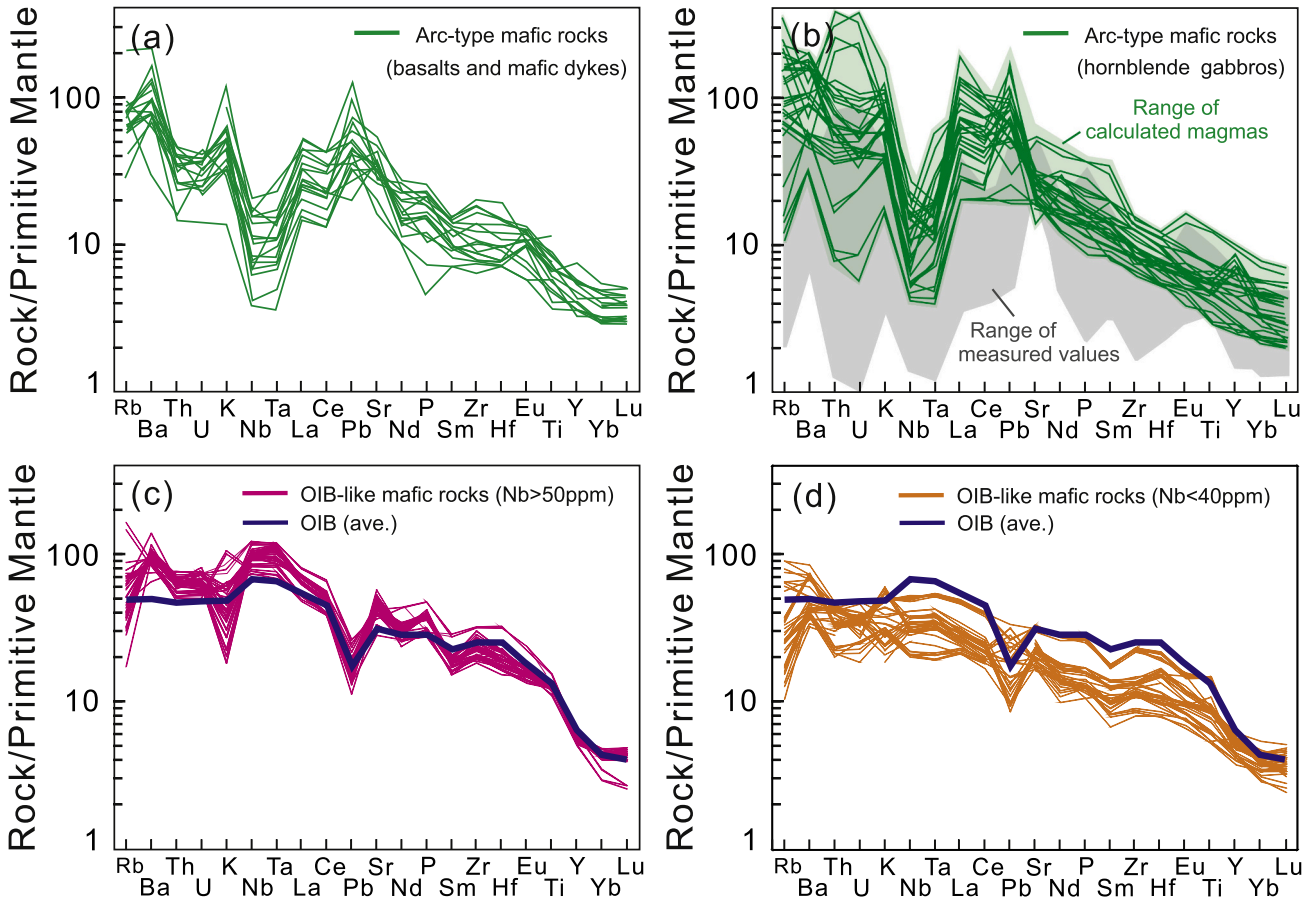

Fig. 4. Primitive mantle (PM)-normalized REE patterns of Cretaceous mafic rocks in SE China. Normalized values of primitive mantle are from Sun and McDonough (1989).

The mantle wedge above a subducted slab can be enriched by the addition of (1) aqueous fluid released from the subducting slab (Nichols et al., 1994; Hanyu et al., 2006, 2) silicate melt derived from the subducted sediment and oceanic crust (e.g., Defant and Drummond, 1990; Churikova et al., 2001; Elburg et al., 2002; Woodhead et al., 2001); and (3) the subducted oceanic mélange, which represents a mixture of subducted sediments, altered oceanic crust (AOC) and ultramafic matrix (e.g., Castro et al., 2010; Behn et al., 2011; Marschall and Schumacher, 2012; Parolari et al., 2018; Gómez-Tuena et al., 2018b; Errázuriz-Henao et al., 2019).

Because fluid and melt released from the subducted slab show distinct geochemical behaviors in some elements, so the compositional change of these elements and their ratios can be applied to decipher the respective contribution of fluid and melt to the enrichment of depleted mantle wedge (e.g., Woodhead et al., 2001; Hanyu et al., 2006). For instance, the concentrations of fluid-mobile elements such as LILEs (e.g., K, Rb, Sr, and Ba) and Pb are enriched in the aqueous fluids, whereas the contents of fluid-immobile elements like LREEs, Th, and HFSEs (e.g., Zr, Hf, Nb, and Ta) are low. By contrast, the silicate melt of the subducted sediments should contain high contents of incompatible elements like Th, LREEs, and LILEs since these elements are enriched in pelagic and terrestrial sediments (e.g., Plank, 2014). Accordingly, subduction-related magmas derived from fluid-metasomatized mantle sources can be distinguished from those derived from melt-modified source regions in the LILE/LREE, LILE/HFSE, and LILE/Th ratios (Spandler and Pirard, 2013).

In the case of the Cretaceous arc magmas in SE China, subducted sediment is the most likely candidate to transport the "crustal" geochemical signatures into the mantle wedge. The involvement of a subducted sediment component in these arc mafic rocks can be tracked by trace element diagrams such as Th/Sm versus Th/Ce and Th/Yb versus Ba/La (e.g., Plank, 2014; Woodhead et al., 2001; Zhang et al., 2019). Also, their Sr—Nd isotopic compositions depart from typical depleted mantle values, which suggests the involvement of an enriched component that could be linked to the subduction flux potentially in the form of subducted sediments (Fig. 6a). This is consistent with some modern subduction-related volcanic rocks (e.g., SW Japan, Banda and Lesser Antilles), which also have such crust-like Sr-Nd-Pb isotope compositions and have been widely interpreted in terms of variable contribution from the subducted sediments (e.g., White and Dupré, 1986; Shimoda et al., 1998; Nebel et al., 2011). Furthermore, the arc-type mafic rocks in SE China have low Lu/Hf ratios regardless of the wide ranges of Th/La and Th/Yb, plotting in the field of continental arc magmas from the western Pacific subduction zone (Zhao et al., 2019, Fig. 7a and b). This is also consistent with their relatively high Zr/Nb ratios (Table 1 and Fig. 2d), which suggest the involvement of continental detritus with accessory zircon in a continental arc (e.g., Vervoort et al., 1999).

Because some mafic rocks in SE China show crystal accumulation which may exert an effect to change and offset the "true" Th/REE ratios, the use of Th/REE should be cautious and is hence abandoned here. Nevertheless, previous studies have also demonstrated that a combination of whole-rock Hf and Nd isotope data with some incompatible trace element ratios (e.g., Ba/Nb and Ba/La) that are insensitive to crystal accumulation, is feasible to investigate the metasomatic agent and to estimate the proportion of subducted sediment (e.g., Guo et al., 2016). In order to better estimate the proportion of the subducted sediment component and possible enrichment mechanism (fluid via melt) in the

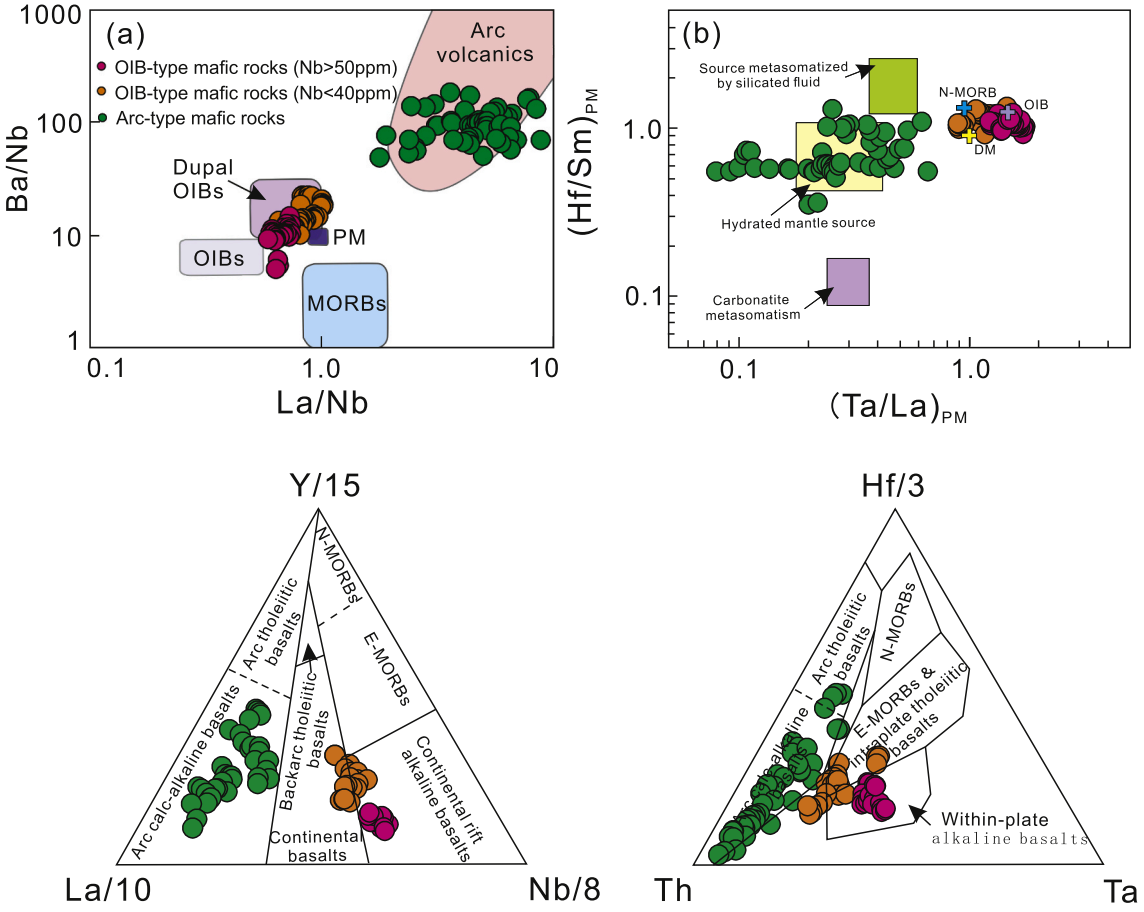

Fig. 5. Plots of La/Nb versus Ba/Nb (a), $(Ta/La)_{PM}$ versus $(Hf/Sm)_{PM}$ (b, La Flèche et al., 1998), La/10-Nb/8-Yb/15 and Th-Ta-Hf/3 Ta/Yb (Li et al., 2015) diagrams, showing the geochemical difference between the Cretaceous OIB-like and arc-type mafic rocks in SE China. The subscript 'PM' denotes primitive mantle normalization.

mantle wedge, we assume that the depleted mantle has: Ba = 4 ppm, Nb = 0.3 ppm, La =0.4 ppm, Nd = 1 ppm, Hf = 0.2 ppm, $\varepsilon_{Nd}(t) = +10$ and $\varepsilon_{Hf}(t) = +17$ and the subducted sediment component has: Ba = 786 ppm, Nb = 9 ppm, La = 29 ppm, Nd = 28 ppm, Hf = 3 ppm, $\varepsilon_{Nd}(t) = -8$ and $\varepsilon_{Hf}(t) = -10$ (Workman and Hart, 2005; Plank and Langmuir, 1998; Guo et al., 2015). During the dehydration of sediment, the dehydration volume is assumed to be 0.02 and the elemental mobilities for Ba, Nb, La, Nd and Hf are assumed to be 8, 0.5, 3, 3 and 0.5, respectively; the partition coefficients of Ba, Nb, La, Nd and Hf are respectively assumed to be 0.05, 0.05, 0.1, 0.05 and 0.2 during sediment melting (Hanyu et al., 2006; Guo et al., 2016; Zhang et al., 2019). Batch melting mode is used for calculation of the elemental concentrations in the sediment-melt. The assumed melting degree of the subducted sediment is ~50%. Two-component mixing modelling is performed and the results are shown in Fig. 7c-g.

The modelling results demonstrate that the source for the majority of arc-type mafic rocks in SE China was enriched by a variable proportion (3–5%) melts derived from the subducted sediments (Fig. 7c-g), except for some arc basalts from Xuantandi and mafic dykes from Tulin that have much higher Ba/La ratios (Table S1), which indicate variable involvement of metasomatic fluids in their melting sources.

5.2. Origin of the high-Nb basalts

High-Nb basalts usually occur in intraplate settings such as continental rifts and oceanic plateaus or islands under lithospheric extension and/or impact by mantle plume, such as those Cenozoic basalts in circum-Pacific Ocean and late Cretaceous to Cenozoic basalts in northwestern North China Craton (e.g., Zou et al., 2000; Ren et al., 2005; Hoernle et al., 2006; Zeng et al., 2011; Liu et al., 2016a; Dai et al., 2019). The Cretaceous high-Nb basalts also occur in rift basins from SE China interior, indicating their formation in an intracontinental regime.

5.2.1. Magmatic evolution

Basaltic lavas may have experienced continental crustal contamination or assimilation during magmatic evolution. Since the continental crust is characterized by negative Nb—Ta anomalies and positive Pb anomaly in PM-normalized trace element spidergram as well as highly evolved isotopic compositions (Rudnick and Gao, 2014), only if a few per cents of continental crust are added into the mantle-derived magma, the geochemical features of the contaminated melt will be largely changed. Obviously, the high-Nb basalts in SE China have OIB-type trace elemental features, such as the positive Nb and Ta anomalies, high Nb/U (41–59) and Ce/Pb (20–38) and negative Pb anomalies. Also, they show mid-oceanic ridge basalt (MORB)-like Sr-Nd-Pb-Hf isotopic compositions (Fig. 6). All these geochemical features strongly indicate the negligible effect of continental crustal contamination or AFC processes during magmatic evolution (Wang et al., 2003, 2008; Wu et al., 2020; Jia et al., 2020).

The high-Nb basalts in SE China show relatively low Mg # (48–59) and compatible element contents such as Cr (97–336 ppm) and Ni (89–149 ppm), indicating that they have experienced significant fractionation of olivine and clinopyroxene. This is consistent with the positive correlation between MgO and CaO and CaO/Al_2O_3 (Fig. 8a and Table S1). Although there lacks a positive correlation between MgO and Al_2O_3 (not shown), the broad correlation between Sr and MgO indicates

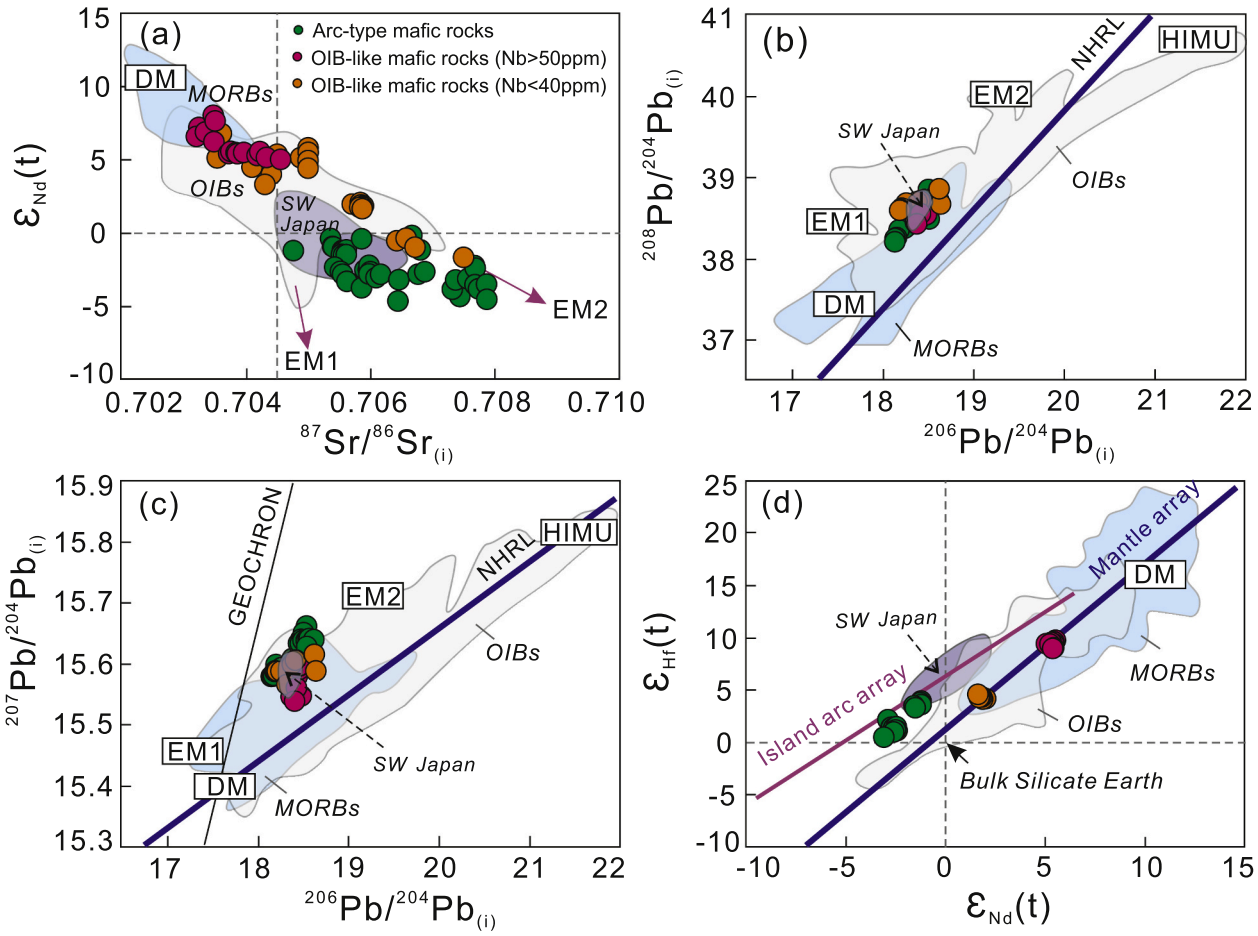

Fig. 6. Sr-Nd-Pb-Hf isotope compositions of the Cretaceous mafic rocks in SE China. Data sources: DM, HIMU, EM1 and EM2 (Iwamori and Nakamura, 2015; Workman and Hart, 2005). The other data are the same as in Fig. 2.

Table 1
A summary of key trace element and Sr-Nd-Pb-Hf isotopic features of Cretaceous arc-type mafic rocks, high-Nb and low-Nb OIB-like basalts in SE China.

Rock type	Arc-type mafic rock	Low-Nb basalt	High-Nb basalt
Nb (ppm)	1.0–14.6 (ave. 4.5)	14–38 (ave. 25)	51–87 (ave. 68)
Ba/Nb	48–183 (ave. 96)	10–23 (ave. 15)	5–15 (ave. 10)
Th/Nb	0.18–3.55 (ave. 0.77)	0.07–0.18 (ave. 0.13)	0.07–0.09 (ave. 0.08)
Zr/Nb	6.9–28.7 (ave. 17.2)	4.6–8.7 (ave. 6.41)	3.1–4.3 (ave. 3.8)
Nb/U	1–27 (ave. 9)	27–53 (ave. 36)	41–59 (ave. 52)
Ce/Pb	1–20 (ave. 7)	7–28 (ave. 16)	20–38 (ave. 28)
$^{87}Sr/^{86}Sr(i)$	0.70478–0.70732 (ave. 0.70589)	0.70355–0.70749 (ave. 0.70534)	0.70323–0.70455 (ave. 0.70379)
$\varepsilon_{Nd}(t)$	−4.73 ~ −0.20 (ave. -2.46)	−1.68–6.84 (ave. 2.91)	5.03–8.00 (ave. 6.07)
$\varepsilon_{Hf}(t)$	0.47–3.89 (ave. 2.25)	4.15–4.57 (ave. 4.30)	8.94–9.69 (ave. 9.37)
$^{206}Pb/^{204}Pb$ (i)	18.131–18.600 (ave. 18.388)	18.178–18.630 (ave. 18.323)	18.363–18.482 (ave. 18.422)
$^{207}Pb/^{204}Pb$ (i)	15.574–15.660 (ave. 15.617)	15.566–15.615 (ave. 15.590)	15.535–15.596 (ave. 15.568)
$^{208}Pb/^{204}Pb$ (i)	38.194–38.791 (ave. 38.534)	38.575–38.883 (ave. 38.649)	38.410–38.593 (ave. 38.515)

Note: The primitive geochemical data are from Table 1S in an excel format. The values of $\varepsilon_{Hf}(t)$ for high-Nb basalts in the Ji'an basin are from Wu et al. (2020), for the low-Nb basalts in the Wuyi basin are from Zhang et al. (2020), and for the mafic intrusions of Pingtan, Daiqianshan and Quanzhou are from Zhang et al. (2019). Ave. – average.

a role of plagioclase fractionation during the evolution of the high-Nb basalts (Fig. 8d). Since the fractional assemblage of olivine + clinopyroxene + plagioclase has a minor effect on the key geochemical features such as Nb/La ratios and Sr-Nd-Pb-Hf-Os-O isotope compositions (e.g., White, 2015), so we attribute the OIB-like geochemical features of the high-Nb basalts to the source enrichment.

5.2.2. *Nature of the mantle source*

The MORB-like isotopic compositions (e.g., the $\varepsilon_{Nd}(t)$ ranges from +5.0 to +8.0) of the high-Nb basalts in SE China suggest a predominant source from the depleted asthenospheric mantle. However, melting of a pure asthenosphere produces tholeiitic to low-K basalts with trace element features similar to MORBs, which have Nb concentrations much less than 50 ppm (Sun and McDonough, 1989), i.e., high-degree melting produces N-MORB and low-degree melting forms *E*-MORB. Therefore, the OIB-like trace element geochemistry and high $^{187}Os/^{188}Os(i)$ ratios (i.e., relative to mantle, crust has higher Re/Os and develops time-integrated growth of more radiogenic Os) of the high-Nb basalts requires the involvement of another enriched component, e.g., a recycled oceanic slab or an enriched mantle (Wang et al., 2003; Stracke et al., 2003; Wu et al., 2020).

Alternatively, previous studies have suggested that the high-Nb basalts represented the melts of an OIB-type asthenosphere and variably interacted with the enriched subcontinental lithospheric mantle (SCLM) to interpret their Sr-Nd-Pb isotopic variations and Sr—Ba enrichment (Figs. 3a and 6, Wang et al., 2003, 2008). Based on geochemical and Sr-Nd-Pb isotopic studies on the lamproite in Jiangxi Province, Xie et al. (2006) identified an EM-2 (enriched mantle-2) lithospheric mantle in

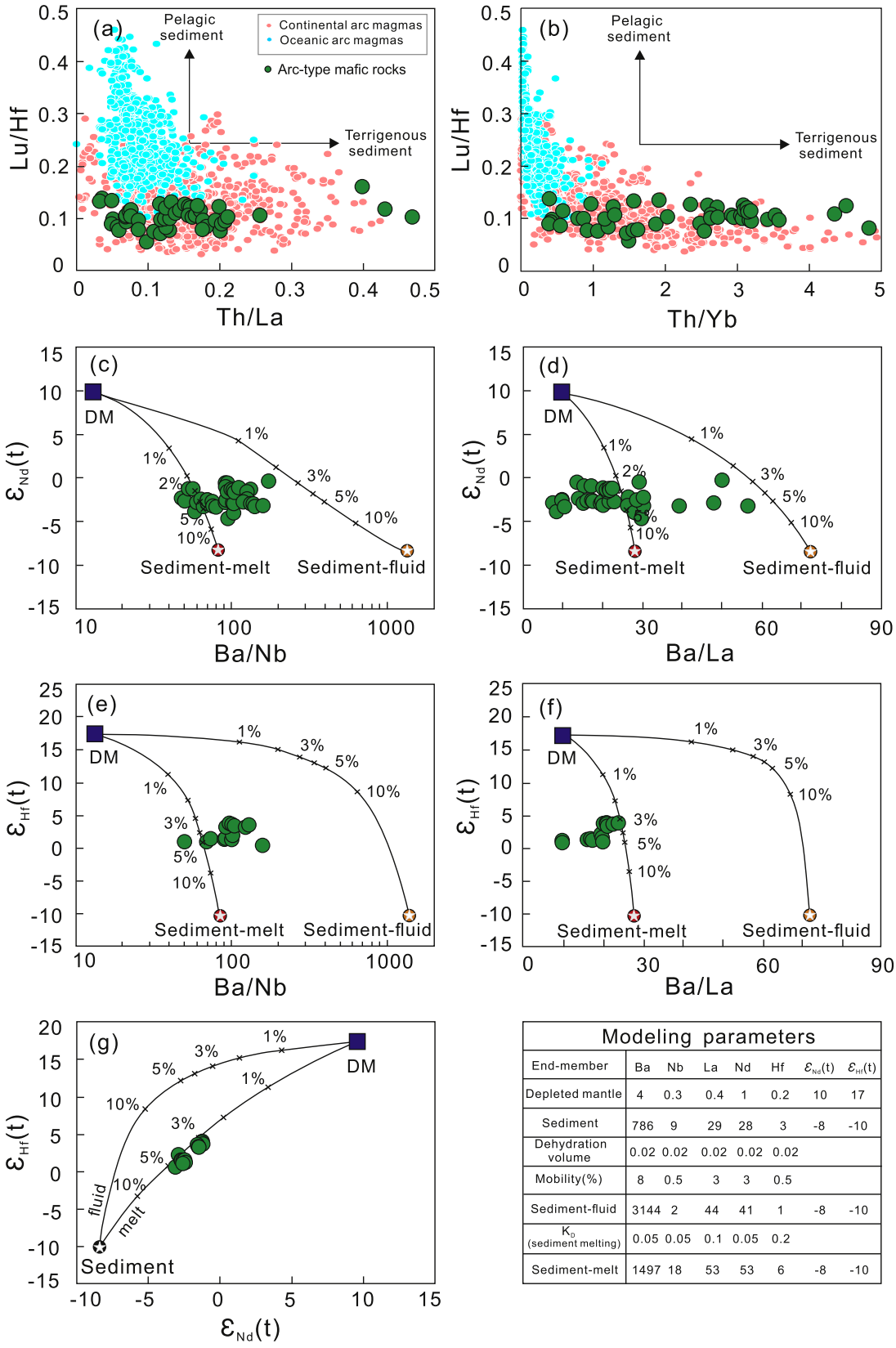

Modeling parameters

End-member	Ba	Nb	La	Nd	Hf	$\varepsilon_{Nd}(t)$	$\varepsilon_{Hf}(t)$
Depleted mantle	4	0.3	0.4	1	0.2	10	17
Sediment	786	9	29	28	3	-8	-10
Dehydration volume	0.02	0.02	0.02	0.02	0.02		
Mobility(%)	8	0.5	3	3	0.5		
Sediment-fluid	3144	2	44	41	1	-8	-10
K_D (sediment melting)	0.05	0.05	0.1	0.05	0.2		
Sediment-melt	1497	18	53	53	6	-8	-10

Fig. 7. Plots of Th/La and Th/Yb versus Lu/Hf (a and b, Zhao et al., 2019), Ba/Nb versus $\varepsilon_{Nd}(t)$ (c), Ba/La versus $\varepsilon_{Nd}(t)$ (d), Ba/Nb versus $\varepsilon_{Hf}(t)$ (e), Ba/La versus $\varepsilon_{Hf}(t)$ (f) and $\varepsilon_{Nd}(t)$ versus $\varepsilon_{Hf}(t)$ (g) of Cretaceous mafic intrusions (after Guo et al., 2016 and Zhang et al., 2019). Detailed calculation parameters of endmember components and data processing are the same as those in Zhang et al. (2019). Data sources for the continental arcs (Kamchatka and Honshu) and oceanic arcs (Izu-Bonin-Mariana arcs) are collected from the database GEOROC (http://georoc.mpch-mainz.gwdg.de/georoc). During the dehydration and melting of the subducted sediment, the element mobilities are from Alzawa et al. (1999) and the partition coefficients are from Hermann and Spandler (2008).

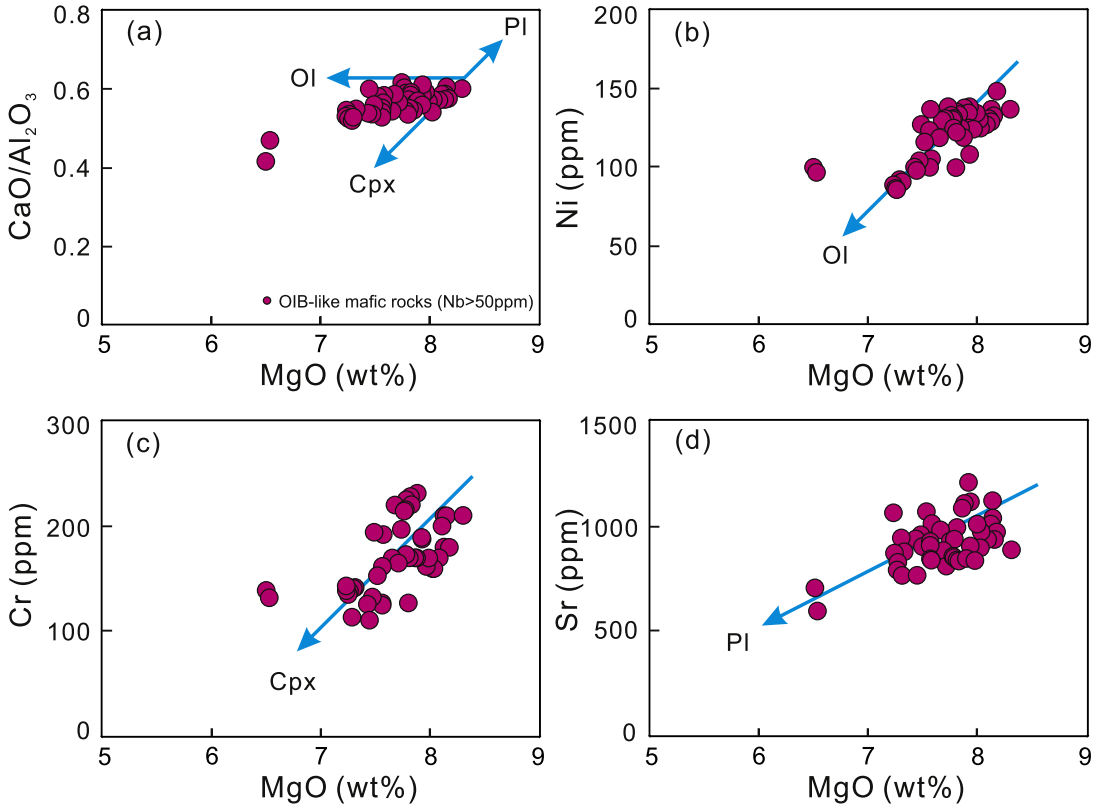

Fig. 8. MgO versus CaO/Al_2O_3 (a), Ni (b), Cr (c) and Sr (d) plots to show the possible fractional phases of high-Nb basalts during magmatic evolution. Data sources are from Table S1.

the Cretaceous. These lamproites are significantly enriched in LILEs and LREEs, depleted in HFSEs (e.g., Nb/La = 0.31–0.47), and also show enriched Sr ($^{87}Sr/^{86}Sr(i)$ = 0.7077–0.7130) and Nd ($\varepsilon_{Nd}(t)$ = −2.1 to −10) isotopic signatures. Although the asthenosphere has depleted Sr—Nd isotopic signatures ($^{87}Sr/^{86}Sr(i) < 0.703$ and $\varepsilon_{Nd}(t) > 10$), numerical studies indicate that it has Nb/La < 1.2 (e.g., Sun and McDonough, 1989; Workman and Hart, 2005). During the fractional crystallization of olivine + clinopyroxene +/− plagioclase and mantle melting, Nb/La fractionation can be negligible, so the involvement of an enriched SCLM represented by the lamproite must result in a decrease of Nb/La of the hybridized melts from the asthenosphere. Therefore, the higher Nb/La (1.37–1.73) ratios of the high-Nb basalts argue against the incorporation of an enriched SCLM either as a contaminant during the passage of the lithosphere or as an enriched component through lithosphere-asthenosphere interaction.

Recently, Wu et al. (2020) discovered low-$\delta^{18}O$ olivine in some high-Nb basalts from the Ji'an basin and attributed to the involvement of a gabbroic oceanic crust that had been undergone high-temperature hydrothermal alteration. This is consistent with the Sr—Ba enrichment in all high-Nb samples in SE China, since Sr and Ba are fluid-mobile elements and can be easily absorbed in the altered minerals such as chlorite, kaolinite and serpentine during seawater alteration (e.g., Kogiso et al., 1997). In addition, the strong Pb depletion and high Ba/Nb and Ba/Th in the high-Nb rocks require the incorporation of the altered gabbroic oceanic crust that had experienced extensive dehydration. Furthermore, the relationships of Nb/Zr versus Ba/Zr and of Nb/Y versus Rb/Y (Fig. 9a and b) indicate a dominated source enrichment by slab melt. Accordingly, we assume an AOC component to represent the end-member of recycled mafic oceanic crust and GLOSS-II to represent the end-member of sediments (Hauff et al., 2003; Plank, 2014 and references therein), which experienced dehydration and melting. Through assuming the other reasonable parameters (Fig. 9), we conduct a three-component mixing modelling to show the respective contribution of each end-member component. Further trace element-isotopic modelling suggests that the mantle source of high-Nb basalts could be formed through addition of 1–5% slab melts into the depleted asthenospheric mantle, with the melt predominant (>70%) from the altered oceanic crust (Fig. 9c-e).

At the other hand, we recalculate the primitive magma compositions of the high-Nb basalts from the Ji'an and Liuyang basins through addition of olivine into the melt. The results suggest that their source lithology was probably composed of silica-deficient pyroxenite (Fig. 10, Herzberg, 2011; Wu et al., 2020), which was formed through interaction between the melts from the dehydrated gabbroic oceanic crust and the mantle peridotite at high temperature (e.g., Zanetti et al., 1999; Sobolev et al., 2007; Straub et al., 2011; Lambart et al., 2012). Melting of the Si-poor lithology produced the SiO_2-undersaturated and strongly alkaline magmas in composition (Hirschmann et al., 2003; Kogiso et al., 2003). This is consistent with the high-Nb basalts that contain standard olivine + nepheline in normative mineral (CIPW) calculation. Finally, the low $\delta^{18}O$ preserved in olivine phenocrysts and the estimated slab age (<300 Ma) from the radiogenic whole-rock Os and Pb compositions in the Ji'an high-Nb basalts require the involvement of a recently recycled slab, probably represented by the subducted paleo-Pacific oceanic plate (Wu et al., 2020).

5.3. *Origins of the low-Nb basalts*

The low-Nb basalts in SE China generally show geochemical features transitional between the high-Nb basalts and arc-type mafic rocks. Compared with the high-Nb basalts, the distribution of low-Nb basalts is more widespread, e.g., from the coastal region like the Wuyi basin to the continent interior such as the Liuyang basin. These rocks also span large compositional and isotopic variations (Table 1), suggesting complex magmatic evolution and/or source heterogeneity in their origin.

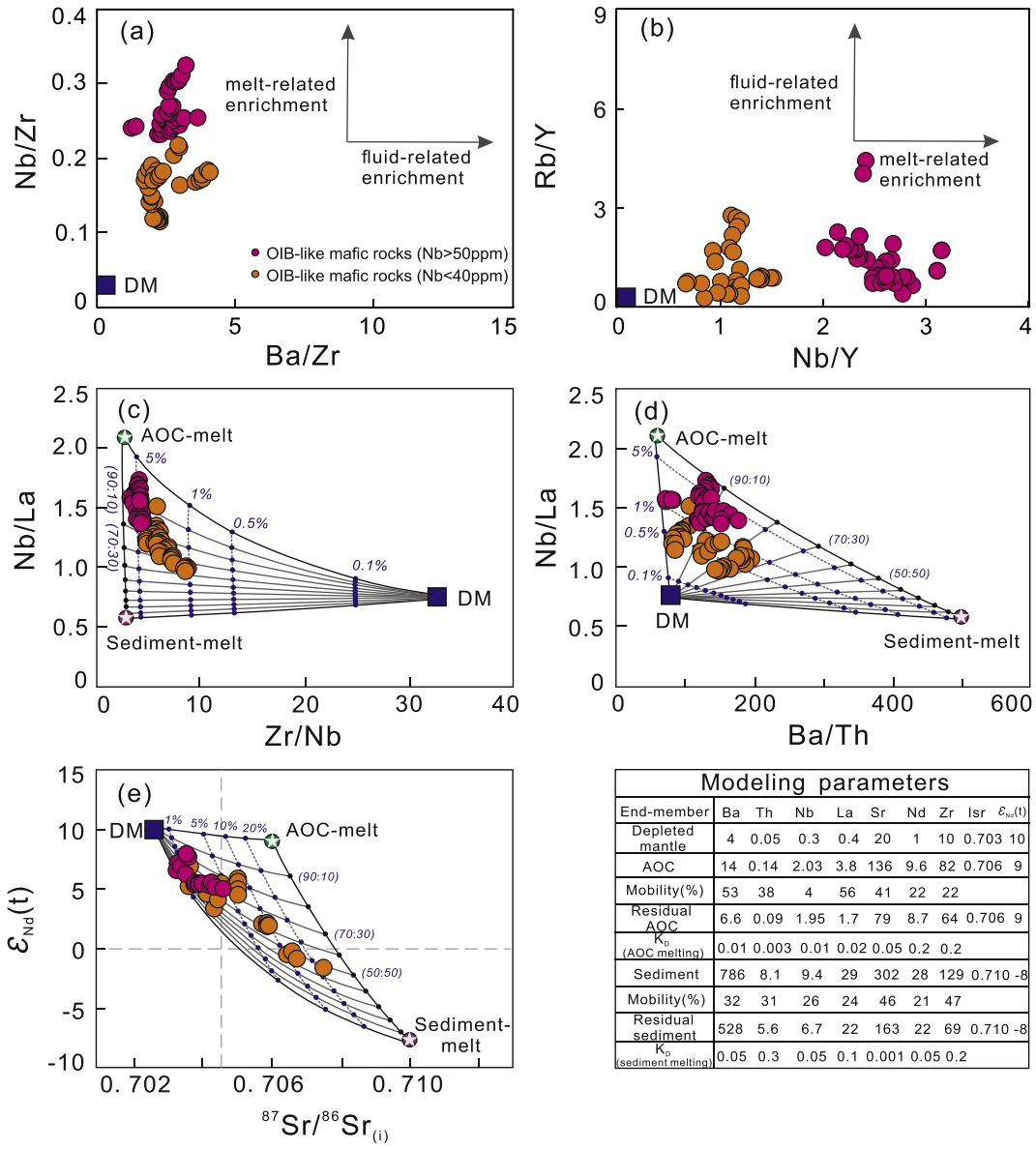

Modeling parameters

End-member	Ba	Th	Nb	La	Sr	Nd	Zr	Isr	$\varepsilon_{Nd}(t)$
Depleted mantle	4	0.05	0.3	0.4	20	1	10	0.703	10
AOC	14	0.14	2.03	3.8	136	9.6	82	0.706	9
Mobility(%)	53	38	4	56	41	22	22		
Residual AOC	6.6	0.09	1.95	1.7	79	8.7	64	0.706	9
K_D (AOC melting)	0.01	0.003	0.01	0.02	0.05	0.2	0.2		
Sediment	786	8.1	9.4	29	302	28	129	0.710	-8
Mobility(%)	32	31	26	24	46	21	47		
Residual sediment	528	5.6	6.7	22	163	22	69	0.710	-8
K_D (sediment melting)	0.05	0.3	0.05	0.1	0.001	0.05	0.2		

Fig. 9. Ba/Zr versus Nb/Zr (a), Nb/Y versus Rb/Y (b), Nb/La versus Zr/Nb (c) and Ba/Th (d) and $^{87}Sr/^{86}Sr(i)$ versus $\varepsilon_{Nd}(t)$ diagrams to show the source enrichment by slab melt. The modelling method in (c) and (d) was reported in Liu et al. (2016a) and that in (e) was reported in Zhang et al. (2020). The calculation parameters are listed in the figure. See details in the text.

5.3.1. Magmatic evolution

Similarly, before constraining the source nature of the low-Nb basalts in SE China, we first assess the potential influence of open-system processes such as crustal contamination, mixing and AFC processes during its passage through the continental crust.

The narrow variations in Sr-Nd-Pb isotopic compositions in a single volcanic basin (Fig. 11 and Table S1) suggest that crustal contamination or AFC processes played an insignificant role during magmatic evolution. For instance, the dolerite sills and basalts from the coastal SE China show narrow variations in Sr-Nd-Pb-Hf isotopic compositions and identical Sr and Pb isotope compositions between plagioclase and bulk rock, precluding an important role of crustal contamination or AFC processes (Zhang et al., 2020). A similar case is observed in the basaltic lavas in Hengyang basin (Meng et al., 2012) and along the Jiangshan-Shaoxing Fault zone (Qin et al., 2019). Previous studies have suggested that a mafic magma with signatures of crustal assimilation generally has La/Nb > 1.5 and La/Ta > 22 (e.g., Ali et al., 2013), quite different from the low-Nb basalts which have relatively low La/Nb (0.66–1.02) and La/Ta (11.5–18.7) ratios. Finally, the significant role of crustal contamination or AFC processes can also be ruled out in accordance with the variation trends between La/Nb and Th/Nb, Nb and Nb/U, SiO_2 and $^{87}Sr/^{86}Sr(i)$ and MgO and $\varepsilon_{Nd}(t)$ in each location (Fig. 11).

Because of the coeval occurrence of low-Nb and high-Nb basalts in both the Ji'an and Liuyang basins, it is also necessary to investigate the possible genetic relationship between these two rock types. Although the low-Nb basalts generally have slightly lower Nd and higher Sr isotopic compositions than the high-Nb basalts (Wu et al., 2020; Wang et al., 2003, 2008; Jia et al., 2020), which might suggest a role of open-system evolution, the compositional gaps in SiO_2, P_2O_5, Nb, La concentrations as well as Nb/La and Nb/U ratios between these two rock types in each basin (Table S3) argue against a relationship of magmatic differentiation either in close-system or open-system processes.

The low-Nb basalts have relatively low MgO (5.2–9.4 wt%), Mg# (42.8–63.1), Cr (38–287 ppm) and Ni (40–176 ppm), indicating a significant role of a fractional assemblage of olivine + clinopyroxene. In contrast, the lack of negative Eu and Sr anomalies respectively in chondrite-normalized REE patterns and PM-normalized trace element spidergrams suggest an insignificant plagioclase fractionation (Fig. 4d).

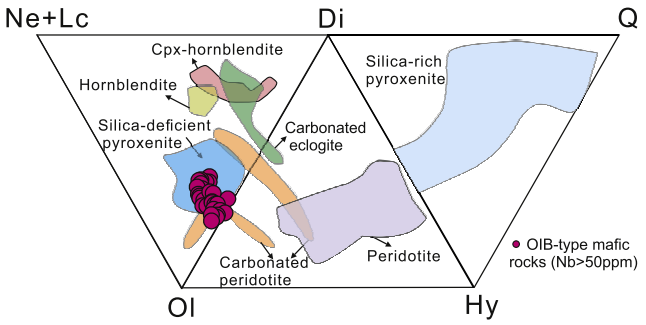

Fig. 10. CIPW normalization plotted in Ne + Lc (nepheline + leucite), Ol (olivine), Di (diopside), Hy (hypersthene), Q (quartz) space (Thompson and Gibson, 2000). Melt compositions in a range of partial melting experiments on various sources, including: hornblendite, clinopyroxene (Cpx) - hornblendite, carbonated peridotite, carbonated eclogite, silica-deficient pyroxenite, silica-rich pyroxenite, and peridotite. All data were calculated using the assumption that 10% of the total iron as Fe_2O_3.

In summary, the low-Nb basalts experienced a close-system magmatic evolution, during which fractionation of olivine and clinopyroxene was predominant.

5.3.2. *Nature of mantle source*

The low-Nb basalts show geochemistry transitional between the high-Nb basalts and arc-type mafic rocks, suggesting that their mantle source was also transitional. Nevertheless, it is necessary to evaluate the possible role of the SCLM in their origin.

As discussed earlier, there existed an enriched SCLM beneath SE China. Interaction between the high-Nb basalts and the enriched mantle may result in the decrease of Nb (Nb/La) and $\varepsilon_{Nd}(t)$ but the increase of $^{87}Sr/^{86}Sr(i)$ and Ba/Nb. For simplicity, we assume that the enriched SCLM has about two times of Sr (42 ppm) and Nd (2.7 ppm) as the primitive mantle and $\varepsilon_{Nd}(t) = -10$ and $^{87}Sr/^{86}Sr(i) = 0.710$, respectively (Sun and McDonough, 1989; Xie et al., 2006; White, 2015). The primary magma of high-Nb basalts are assumed as: Sr = 850 ppm and Nd = 74 ppm, $\varepsilon_{Nd}(t) = +8$ and $^{87}Sr/^{86}Sr(i) = 0.7035$, as represented by the high-Nb basalt from the Liuyang basin (Wang et al., 2003, 2008). A simple binary mixing between the high-Nb basalt and SCLM is modelled. The results indicate that mixing of 50% SCLM into the high-Nb basalt can produce a decrease of $\varepsilon_{Nd}(t)$ by 0.6 unit and an increase of $^{87}Sr/^{86}Sr(i)$ by 0.0003. Such a contaminated basalt should have very high MgO similar to picrite and contain abundant mantle xenoliths, inconsistent with the petrologic and geochemical observations in the low-Nb basalts.

An alternative hypothesis suggests the enriched SCLM as a source component of the low-Nb basalts. Previous studies suggest that melts derived from the enriched SCLM are strongly alkaline and SiO_2-undersaturated such as lamproite and trachybasalt (e.g., Foley, 1992). If the low-Nb basalts had been derived from a mixture of the enriched SCLM and the metasomatized asthenosphere, the primitive magma must be SiO_2-undersaturated and strongly alkaline. However, most of the low-Nb basalts are weakly alkaline and SiO_2-saturated with normative quartz and/or hypersthene in CIPW calculation (e.g., Meng et al., 2012; Li et al., 2018). Accordingly, the contribution of enriched SCLM to the formation of the low-Nb basalt should be also minor.

Following the aforementioned facts, we consider that the enriched source component of the low-Nb basalts was represented by the subducted sediments, which might have experienced variable degrees of dehydration and melting during the downgoing subduction. For instance, Zhang et al. (2020) discovered the light Ca isotope compositions (Ca isotope fractionation is strong at the Earth's surface and calcic sediments generally have much lower $\delta^{44/40}Ca$ than mantle, Fantle and Tipper, 2014) of the dolerite sill (corresponding to low-Nb basalt) from the Wuyi basin, indicating the involvement of Ca-rich sediment in the

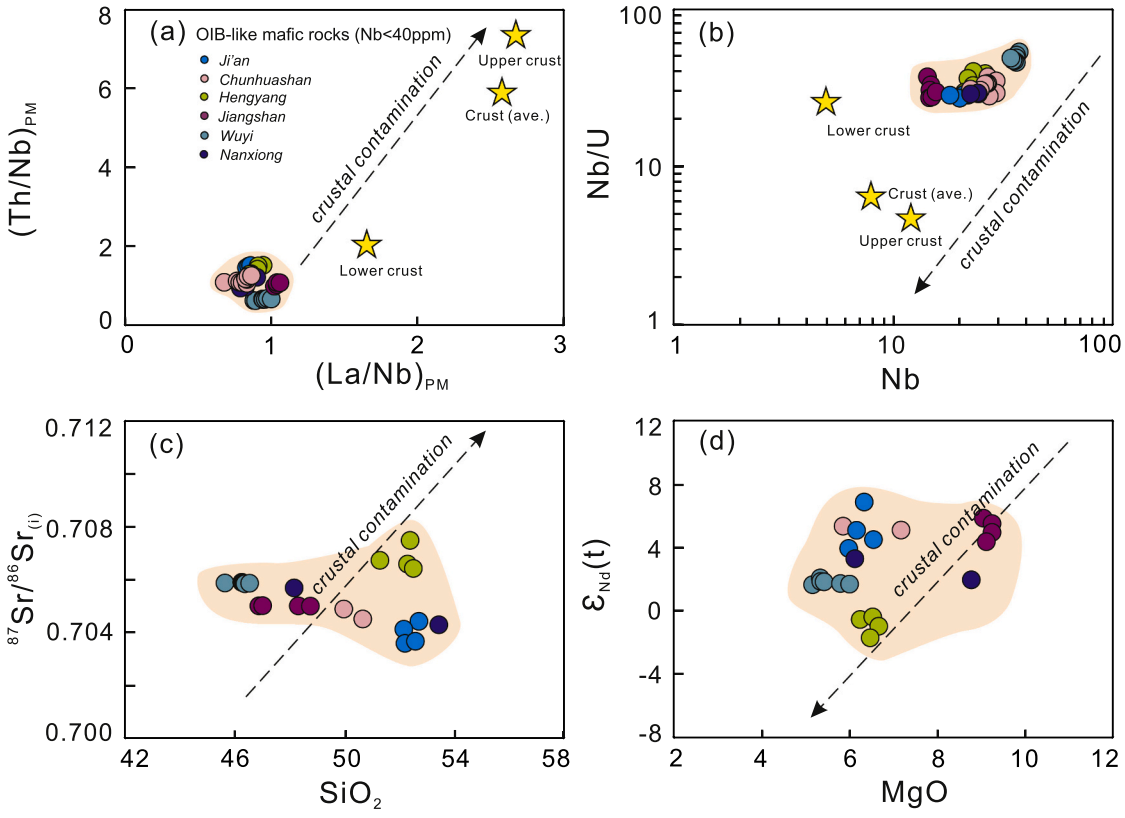

Fig. 11. $(La/Nb)_{PM}$ versus $(Th/Nb)_{PM}$ (a), Nb versus Nb/U (b), SiO_2 versus $^{87}Sr/^{86}Sr(i)$ (c) and MgO versus $\varepsilon_{Nd}(t)$ (d) diagrams of low-Nb basalts to show the possible role of crustal contamination. The compositions of average crust, lower and upper crust are from Rudnick and Gao (2014). The other data are from Table S1.

source. Also, some low-Nb samples show positive Pb anomalies, which indicates the incorporation of a recycled crustal component in the source. Compared to the enriched SCLM, the terrestrial sediments have much higher Sr and Nd and evolved isotopic compositions, and their derivative melts are felsic in composition as well. The relationships of Ba/Zr versus Nb/Zr and Nb/Y versus Rb/Y also confirm the dominated melt metasomatism in the mantle source of the low-Nb basalts (Fig. 9a and b). Interaction of sediment melt with the mantle peridotite will form SiO_2-rich pyroxenite (e.g., Sobolev et al., 2007; Straub et al., 2011; Lambart et al., 2012, 2016). Melts derived from the Si-saturated pyroxenite can be calk-alkaline and SiO_2-oversaturated (e.g., Lambart et al., 2009, 2016; Herzberg, 2011). Interaction between the Si-saturated and Si-undersaturated melts can form the weakly alkaline basalts like the low-Nb basalts in SE China (e.g., Ren et al., 2005).

In order to test the hypothesis, we also conduct trace element and isotopic modelling calculation on the low-Nb basalts, as shown in Fig. 9c-e. Results inferred from the Nb/La versus Zr/Nb and Ba/Th and Sr—Nd isotopic compositions show that the mantle source of the low-Nb basalts can be best explained by addition of slab melt with a ratio of AOC-melt/sediment-melt range from 80:20 to 50:50 into the depleted asthenospheric mantle (Fig. 9). Considering the occurrence of contemporaneous oceanic plate subduction and the close space-time relationship between the early Cretaceous OIB-type and arc-type magmatism, such metasomatic melts were most probably derived from the subducting paleo-Pacific slab.

6. Geodynamic implications

6.1. Numerical simulation of slab melting

The combined geochemical data of high-Nb and low-Nb basalts indicate that they were derived from an asthenospheric mantle that had been enriched by melts derived from the subducting paleo-Pacific slab. However, the global ranges of top-slab geotherm are far below the MORB solidus (Syracuse et al., 2010), which makes it difficult to melt the dehydrated oceanic crust as inferred from the OIB-like magmas, especially for the high-Nb basalts in SE China. This implies a unique geodynamic process for the asthenosphere-slab interaction during the generation of OIB-like basalts in the region.

To quantify the geodynamic mechanism for slab melting, we perform two-dimensional numerical modelling by using a thermo-mechanical coupled numerical code I2VIS (Gerya and Yuen, 2003b) based on finite-difference and marker-in-cell techniques. The following three governing equations (i.e., the mass, momentum and energy conservation equations) are solved in the numerical code,

$$\frac{\partial v_i}{\partial x_i} = 0$$

$$\frac{\partial \sigma'_{ij}}{\partial x_j} - \frac{\partial P}{\partial x_i} = -\rho g_i$$

$$\rho C_p \frac{DT}{Dt} = \frac{\partial}{\partial x_i}\left(k\frac{\partial T}{\partial x_i}\right) + H_r + H_s + H_a + H_L$$

where v is velocity, $\sigma'$is the deviatoric stress tensor, P is the total pressure (mean normal stress), ρ is density, g is gravitational acceleration, C_p is heat capacity, T is temperature, k is thermal conductivity, H is internal heating, H_s is shear heating, H_a is adiabatic heating, H_r is radioactive heating with a constant value for each rock, H_L is latent heating included implicitly by increasing the effective heat capacity and thermal expansion of the partially crystallized/molten rocks (Burg and Gerya, 2005), $k = 1.18 + 474/(T + 770)$ for oceanic crust, and $k = [0.73 + 1293/(T + 77)]\exp(0.00004P)$ for oceanic mantle. The rheological parameters in this study were reported in Liao et al. (2017, 2018).

On the basis of petrophysical experimental constraints, the numerical code applied here also encompasses the melting behavior of rock. We assumed a simple linear relationship between the melting percentage F and temperature, as follows:

$$F = 0 \text{ when } T \le T_{solidus}$$

$$F = \frac{T - T_{solidus}}{T_{liquidus} - T_{solidus}} \; when T_{solidus} < T < T_{liquidus}$$

$$F = 1 \text{ when } T \ge T_{liquidus}$$

Where $T_{solidus}$ and $T_{liquidus}$ refer to the solidus and liquidus temperature of rocks, respectively. In this study, the solidus and liquidus temperature (Gerya and Yuen, 2003a) of oceanic crust are as follows:

$$T_{solidus} = 973 - \frac{70400}{P + 354} + 778 \times \frac{10^5}{(P + 354)^2}, when\ P < 1600\ MPa$$

$$T_{solidus} = 935 + 0.0035P + 0.62 \times 10^{-5}P^2, when\ P > 1600\ MPa$$

$$T_{liquidus} = 1423 + 0.105P$$

The initial model setup is shown in Fig. 12. The horizontal width of the model is 500 km and the vertical depth is 400 km. The entire model space is discretized using a regular grid composed of 501 × 401 nodes. The mechanical boundary conditions are everywhere free slip. Initial temperature for the continental lithosphere is linear with a surface temperature of 0 °C and a temperature of 1300 °C at the base. The adiabatic thermal gradient is set to 0.5 °C/km for the asthenospheric mantle. For the oceanic slab, initial temperature is linear with a temperature of 600 °C at the top and a temperature of 1200 °C at the bottom. An initial cold zone above the slab with temperature decreasing from 1000 °C to 600 °C is also set to match the thermal structure of a subducting slab (Stern, 2002 and references therein).

The detailed evolution processes including temperature field and compositional field during a fragmented slab (50 km in width) sinking in the asthenosphere are shown in Fig. 13. When the thickness of the fragmented slab is 60 km and 40 km, only low-degree melting occurs along the fractured surface (Fig. 13a and b). However, once the fragmented slab is thinned to 20 km, the area of partial melting occurs along the fractured surface and lower part of oceanic crust (Fig. 13c). Fig. 14 further shows that melting degree can be up to ~20% along the fractured surface and ~ 10% at the lower part of oceanic crust in the case of a thinned and fragmented slab regardless of the variation of slab width. Our results indicate the slab thickness is the predominant factor to control the melting behavior of dehydrated oceanic crust (Fig. 14). The slab width may enlarge the melting region as the sinking velocity is negatively correlated with the slab width, especially in the early stage (Figs. 14 and 15), during which the fragmentated slab has enough time to be heated in the upper part of asthenosphere. Our results indicate that (1) large-scale partial melting can occur when the fragmented slab is strongly thinned; (2) partial melting mainly occurs along the fractured surface and lower part of the oceanic crust; (3) an increase of the fragmented slab width can obviously increase the melting region of the oceanic crust. Accordingly, large volume of oceanic crust-derived melts can be generated in fragmented slabs and react with the ambient mantle to form the OIB-type mantle source.

Our 2-D numerical modelling results on melting of a dehydrated oceanic crust require the breakdown of a subducting slab, possibly as a consequence of lithospheric delamination, slab breakoff and/or tearing along the rift or weak layer (e.g., Gerya et al., 2004; Rosenbaum et al., 2008; Dai et al., 2020). These dynamic processes might fragment the subducting slab and create a slab window, permitting the asthenospheric upwelling and resultant extensive basaltic magmatism in the SE China interior (Fig. 1; Wu et al., 2020; Zhang et al., 2020).

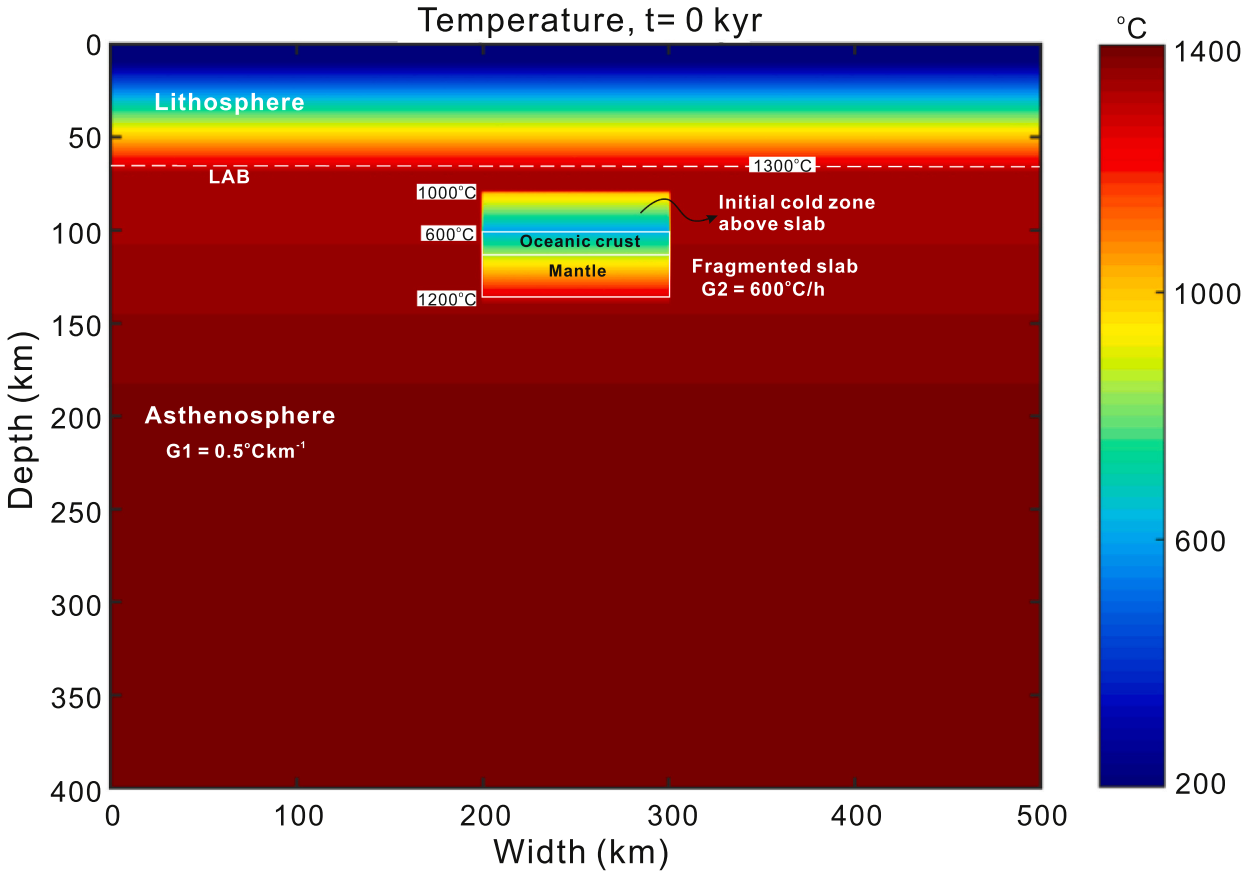

Fig. 12. Initial setup and boundary conditions of the conceptual model of a fragmentated slab. The temperate of the subducting oceanic lithosphere varies from 600 °C at the top to 1200 °C at the base with a constant geothermal gradient (G2 = (1200 °C – 600 °C)/h). Consistent with the geothermal structure of a subduction zone, we also assume a cold zone with a temperate increase from 600 °C at the top to 1200 °C at the bottom above the fragmentated slab. The geothermal gradient of the adiabatic asthenosphere is assumed to be 0.5 °C/km with the top temperature at 1300 °C. See details in the text.

6.2. *Cretaceous subduction and rollback of the paleo-Pacific Oceanic slab*

The birth of the paleo-Pacific Ocean was followed by the breakup of the Pangea in early Jurassic (ca. 190 Ma), when the triple-junction rift among the Izanagi, Farallon and Phoenix Plate was formed (Seton et al., 2012; Müller et al., 2016). The subsequent subduction of the paleo-Pacific Plate beneath the eastern Asian Continent was responsible for the Mesozoic lithospheric deformation, deposition, magmatism and mineralization in SE China (Maruyama et al., 1997).

The Cretaceous arc-type mafic rocks from the coastal region in SE China generally show crust-like isotopic signatures similar to those arc basalts from the SW Japan, Lesser Antilles and Banda arcs (Shimoda et al., 1998; Labanieh et al., 2010; Nebel et al., 2011). A common feature of these modern subduction zones is the predominance of sediment melting in the course of slab subduction, which requires a relatively hot geotherm (e.g., Furukawa and Tatsumi, 1999; Watt et al., 2013). This is consistent with the present thermal state of the involved oceanic plates – the young and hot subducting oceanic lithosphere beneath the SW Japan, Lesser Antilles and Banda arcs (Seton et al., 2012; Müller et al., 2016).

Following the advanced subduction, several lines of evidence indicate rollback of the subducting paleo-Pacific slab and the resultant asthenospheric diapir beneath the SE China (Kincaid and Griffiths, 2003). These include: (1) continuous youthening of the felsic/granitic magmatism from the continental interior to the coastal region of SE China (e.g., Chen and Jahn, 1998; Li et al., 2019; Suo et al., 2019, 2) a rapid increase of magma temperature from ~750 °C in the late Jurassic felsic volcanic lavas and intrusive rocks to more than 830 °C for the late Cretaceous counterparts (e.g., Guo et al., 2012; Li et al., 2014b); (3) the compositional transformation from the hydrous calc-alkaline I-type into water-poor A-type granitoids with obviously increasing K_2O content (Chen et al., 2000; Suo et al., 2019, 4) the migration of depocenter of rifting basins from the continental interior during the early Cretaceous to the coastal region in the late Cretaceous (e.g., Wang et al., 2013; Li et al., 2014a); and (5) the emplacement of OIB-like magmas in the continental interior.

Geochemical modelling results suggest that formation of the Cretaceous OIB-like basalts required melting of the mafic oceanic crust and even the dehydrated oceanic crust of the paleo-Pacific slab, especially for those high-Nb basalts. Interaction between the different components (e.g., the AOC, sediments and ultramafic matrix) of a subducted oceanic mélange and peridotite in the mantle wedge has been also proposed to interpret the coeval arc-type and OIB-like magmatism in modern subduction zones or at convergent plate margins (e.g., Gerya and Yuen, 2003a; Castro et al., 2010; Marschall and Schumacher, 2012; Nielsen and Marschall, 2017; Parolari et al., 2018; Codillo et al., 2018). However, such a hypothesis will be faced with the following difficulty to interpret the systematic geochemical variations from the arc-type to low-Nb and ultimately to high-Nb basalts in SE China. (1) Dehydration melting of an oceanic mafic crust is rather difficult unless the geotherm is high enough (e.g., in the case of subduction of an oceanic ridge or a young (< 40 Ma) oceanic lithosphere, Defant and Drummond, 1990; Peacock et al., 1994; Syracuse et al., 2010). This is inconsistent with the results from plate reconstruction on the paleo-Pacific Ocean, which suggested that the age of the subducted oceanic lithosphere was old than 60 Ma (e.g., Sun et al., 2007; Seton et al., 2012; Müller et al., 2016).

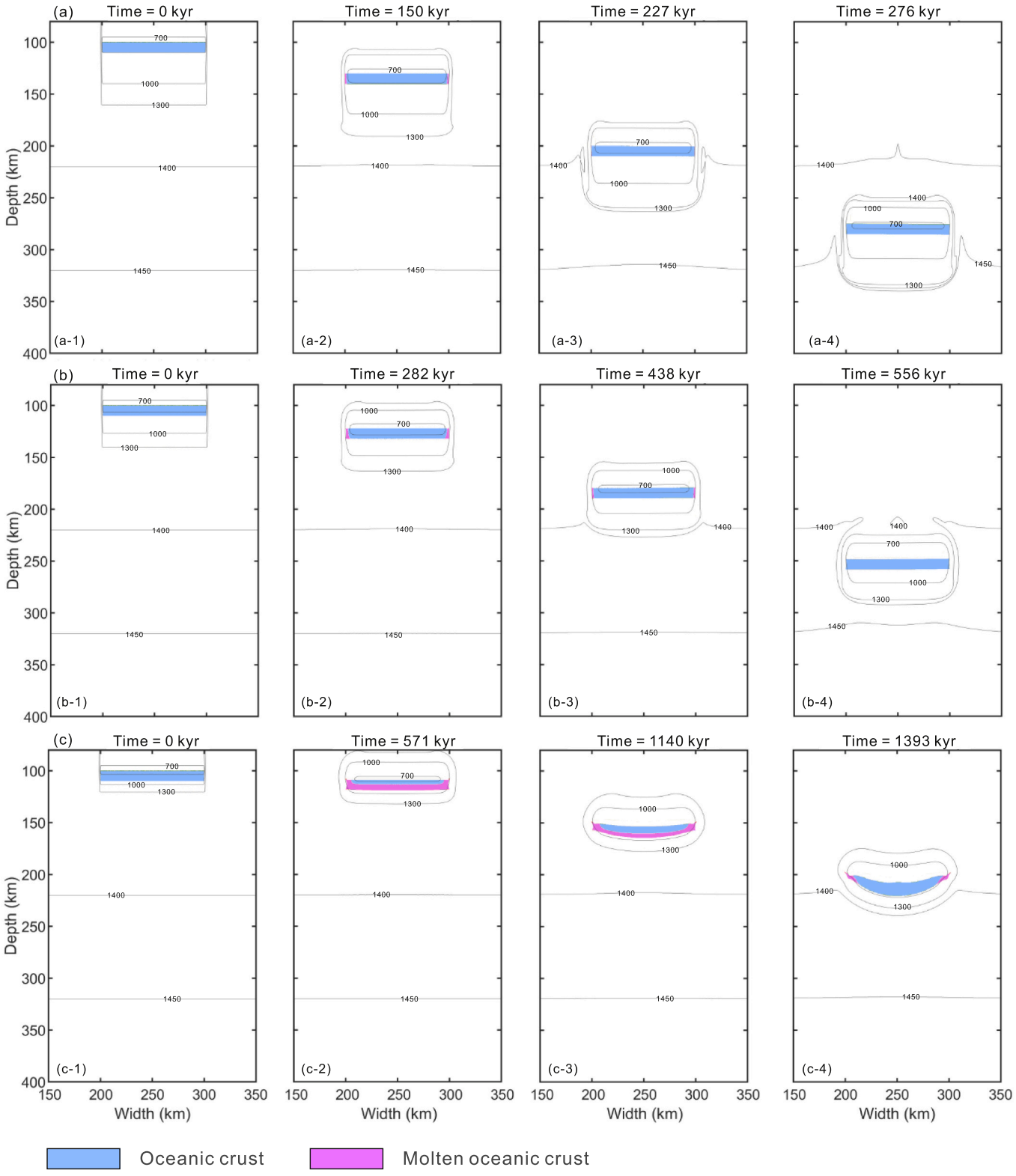

Fig. 13. The evolution of compositional and temperature fields of a fragmentated slab with a width of 100 km at different slab thickness (a – 60 km; b – 40 km; and c – 20 km). The time (t) represents the sinking time in the convective asthenosphere. Melting of the oceanic crust becomes significant when the slab is strongly thinned to 20 km, with the melting region along the torn surface and in the lower part of oceanic crust.

Under the conditions of such 'old' oceanic lithosphere, melting of the mafic components of slab is rather difficult. In contrast, the mélange model requires partial melting of the oceanic mélange at a hot and shallow mantle wedge (Castro et al., 2010; Behn et al., 2011; Marschall and Schumacher, 2012; Nielsen and Marschall, 2017; Codillo et al., 2018). (2) Even if melting of the mafic oceanic crust occurred, e.g., at garnet amphibolite-facies or eclogite-facies conditions, the produced melt should have shown adakitic features (high Sr but low Y and HREE

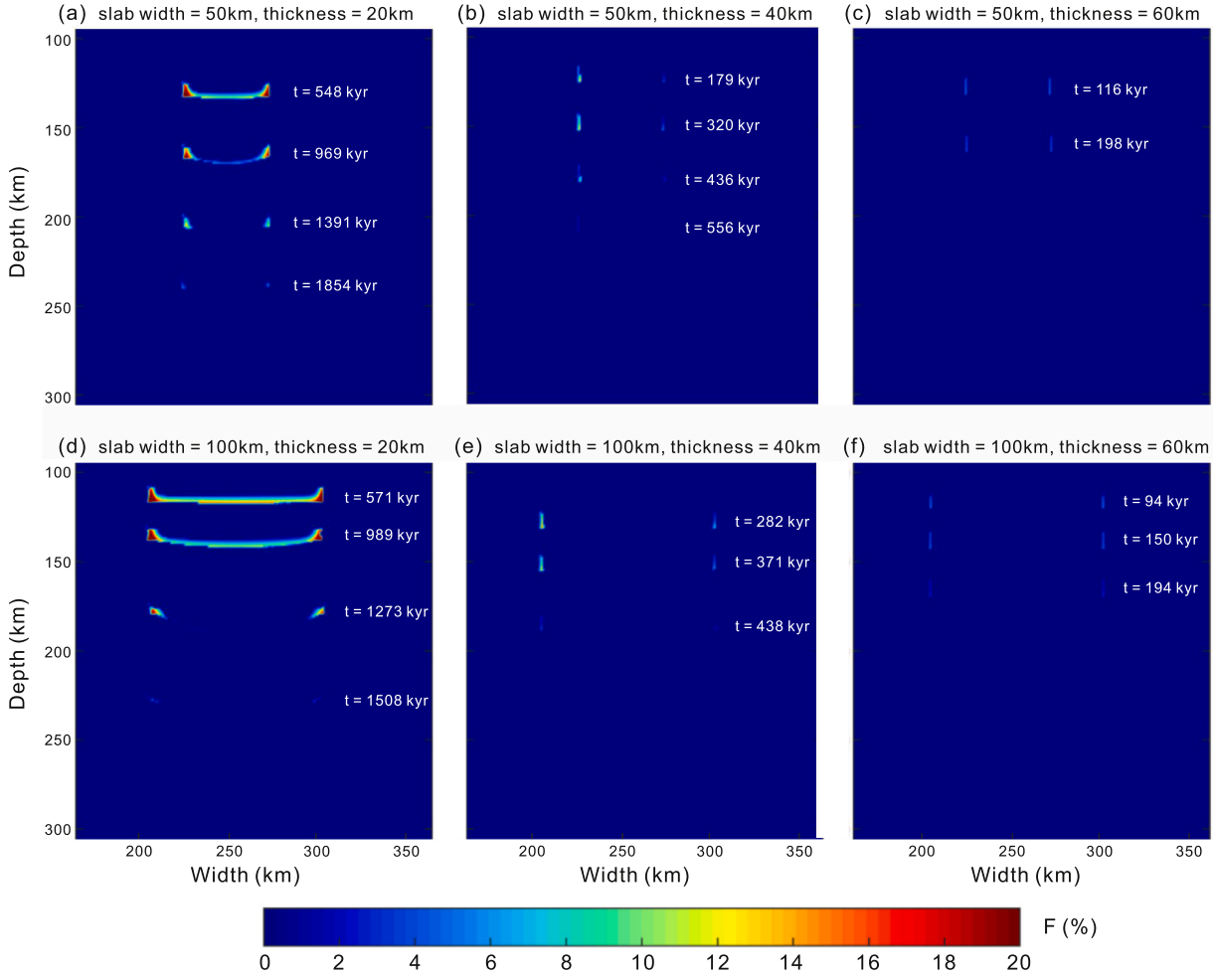

Fig. 14. Melting states of the fragmentated slab during the course of sinking. (a-c) show the melting states of a slab with width of 50 km and (e-f) show the melting states of a slab with 100 km wide. It is obvious that the role of slab thickness is predominant over the melting region and degree of the descending slab, while the slab width may enlarge the melting area.

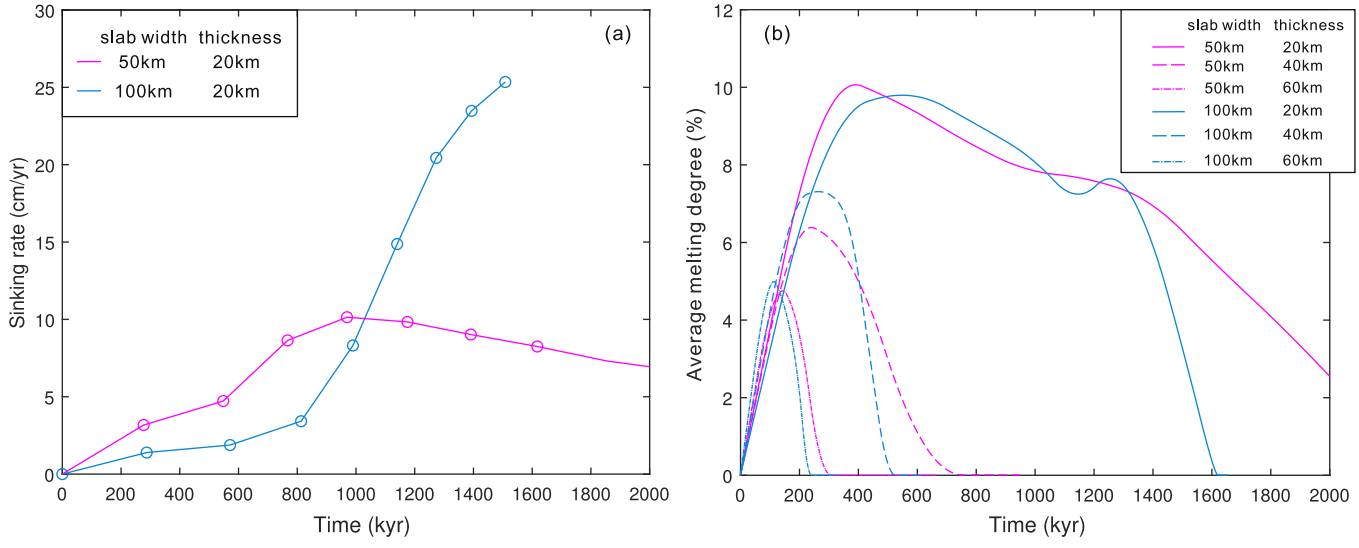

Fig. 15. Relationships of slab sinking time with sinking velocity (a), and melting degree, slab thickness and width (b). In (a), a wider slab sinks more slowly than the narrower slab during the early stage, while it sinks more rapidly at the later stage. In (b), the weighted mean melting degree (F) increases with the thinning of the slab and decays more rapidly for thick slabs, while it is weakly affected by the slab width.

with a residual assemblage of garnet + pyroxene ± amphibole, and MORB-like isotope compositions, Defant and Drummond, 1990). Martin et al. (2005) also defined such adakitic rocks as high-SiO_2 adakite. If the slab melt had interacted with mantle peridotite, and the melts derived from the hybridized mantle would also have shown adakitic features (low-SiO_2 adakite with extremely high Sr, Martin et al., 2005; Guo et al., 2007). Up to now, such Cretaceous adakitic magmas have been rarely reported in SE China, which suggests insignificant melting of the mafic component of the subducted paleo-Pacific Plate during the advanced subduction. (3) Except for the emplacement of dolerite sill and basaltic lavas in the Wuyi basin (~108 Ma), the time of OIB-like magmatism was 10–20 Ma later than the arc-type magmatic activity. Also, the majority of OIB-like magmatism (with the exception of the Wuyi mafic rocks) was located at least 300 km away from the paleo-subduction zone (Fig. 1). These facts are inconsistent with the hypothesis – interaction between subducted mélange and mantle wedge, which predicts the coexistence of contemporaneous OIB-like and arc-type magmatism. Collectively, the hypothesis invoking the interaction between mantle wedge and subducted oceanic mélange might have interpreted the coexistence of arc-type and OIB-like magmatism in the Wuyi basin, while the majority of the OIB-like magmatism do not favor such a tectonic model.

Alternatively, slab tearing or fragmentation can usually be observed through seismic images, e.g., the Yellowstone Park in northwestern U.S.A. and the Tibet Plateau (James et al., 2011; Chen et al., 2015a, 2015b). It can be tectonically related to the development of intracontinental rift system and rifting basins, e.g., in the Tibet Plateau and the northern Apennines of Italy (Chen et al., 2015a, 2015b; Rosenbaum et al., 2008; Rosenbaum and Agostinetti, 2015). Magmatic responses to slab tearing include the coexistence of arc-type and OIB-like magmatism such as in Italy (Rosenbaum et al., 2008) and the coeval SiO_2-undersaturated and SiO_2-oversaturated magmas in western Turkey (Prelević et al., 2015). Although there lacks direct geophysical evidence (it was possibly erased by mantle convection) to support the occurrence of slab tearing beneath SE China during Cretaceous, 3-D seismic images based on multiparameter adjoint tomography suggest that the high-velocity stagnated slabs preserved within the mantle transition zone in SE China may represent the fragmentated paleo-Pacific or Pacific oceanic lithosphere, corresponding to the episodical slab subduction and rollback since late Mesozoic (e.g., Li and van der Hilst, 2010; Chen et al., 2015a, 2015b). In addition, the lithologic assemblage such as in the Ji'an and Liuyang basins (Wang et al., 2003, 2008; Wu et al., 2020; Jia et al., 2020), in which coexistence of high-Nb (SiO_2-undersaturated) and low-Nb (SiO_2-saturated and even oversaturated), and the coeval OIB-like and arc-type dykes/basalts in the Wuyi basin as well (Cui et al., 2011; Zhang et al., 2020), likely suggest fragmentation of the subducting slab. Finally, the development of late Cretaceous rifting basins across the SE China also reflect the deep lithospheric extension as a likely result of rollback and tearing of the subducting paleo-Pacific slab (Wang et al., 2013; Li et al., 2014; Dai et al., 2020).

In accordance with the numerical modelling results (Fig. 13), melting of the dehydrated oceanic crust requires a strongly thinned and/or necked slab, which favors the model of slab tearing or fragmentation. On one hand, previous studies suggested that the dipping angle of the subducting paleo-Pacific slab beneath the SE China was increased from Jurassic to Cretaceous in response to gravitational instability (e.g., Liu et al., 2012; Zhou and Li, 2000). Such a change in dip angle, in fact, could cause rollback of the subducting slab and subsequent extension of the overlying lithosphere (Burchfiel et al., 2018; Nakakuki and Mura, 2013). On the other hand, seismic tomography also reveals that the physical property of subducting oceanic slab is heterogeneous, with faults and weaker zones across the oceanic lithosphere (e.g., Furumura and Kennett, 2005; Miller et al., 2005; Bayrakci et al., 2016). Also, the paleo-Pacific Plate contained microblocks, seamounts and oceanic plateaus (Tejada et al., 1996; Ishikawa et al., 2007), which made the structure of the subducting oceanic lithosphere more complex. Slab tearing is likely to occur within the weaker zone in response to the progressive curvature of a subducting slab (Hale et al., 2010; James et al., 2011; Rosenbaum and Agostinetti, 2015).

Accordingly, we envisage a tectonic hypothesis as illustrated in Fig. 16. Subduction of the relatively hot paleo-Pacific oceanic lithosphere beneath the SE China formed the active continental margin, in which melts from the subducted sediment metasomatized the mantle wedge to form the source of arc-type mafic rocks during 120–110 Ma (a). During 110–70 Ma (b), progressive retreat of the trench and rollback of the subducting slab led to breakdown or fragmentation along the subducted oceanic lithosphere, melting of the torn slab (dehydrated mafic oceanic crust and terrestrial sediment) occurred to enrich the surrounding asthenosphere. Interaction between the melts from the dehydrated oceanic slab with minor or no sediment and the mantle formed the source of high-Nb basalts, whereas reaction between the slab melts with a larger contribution from the sediment and the asthenosphere formed the source of low-Nb basalts. Correspondingly, the depocenter of sedimentary basins migrated from the SE China interior during early Cretaceous to the coastal regions in late Cretaceous (Li et al., 2014).

7. Conclusions

Our new data compilation, sorting and processing of the Cretaceous mafic igneous rocks in SE China indicate a genetic link between the arc-type and OIB-like magmatism in association with subduction and rollback-tearing of the paleo-Pacific Ocean. From the arc-type to low-Nb and ultimately to high-Nb magmas, the increasing Nb concentrations, Nb/LILE and Nb/REE ratios are followed by more depleted Sr-Nd-Pb-Hf isotopic features, reflecting that the slab melting migrated from the upper subducted sediment to the lower oceanic mafic crust. The following conclusions can be summarized:

1. The arc-type basalts and mafic intrusive rocks show that SE China was an active continental margin of the circum-Pacific tectonic domain during Cretaceous. Melting of the terrestrial sediment melt-metasomatized mantle wedge formed the primitive mafic arc magmas, which underwent extensive fractional crystallization and/or accumulation to form the NE-trending arc magmatic belt. The predominant enrichment of the mantle wedge through melting of the subducted sediment reflects a relatively hot subduction zone, which can be comparable with the modern counterparts such as the SW Japan and Less Antilles arcs.
2. The OIB-like basalts and mafic dykes in SE China were derived from the asthenospheric mantle metasomatized by melts from the subducted paleo-Pacific slab. The high-Nb basalts were derived from a pyroxenite-dominated mantle source, which was probably formed through reaction between the melt of dehydrated oceanic crust and the asthenospheric mantle, with minor contribution from the subducted terrestrial sediments. Relative to the high-Nb basalts, a larger amount of melt from the subducted sediments contributed to the mantle source of the low-Nb basalts.
3. Numerical modelling results indicate that melting of the dehydrated oceanic crust within asthenosphere requires a strongly thinned slab, consistent with the contribution of fragmented pieces of recycled crustal component.
4. The geochemical variations from the Cretaceous arc mafic magma in the coastal region to the intracontinental OIB-like basalt in SE China reflect the dynamic transition of the paleo-Pacific Plate from advanced subduction to rollback-tearing, coupled with the formation of rift basins and the migration of the depocenter from the inland during early Cretaceous to the coastal area in late Cretaceous. The heterogeneity of the subducted oceanic lithosphere might be the main controlling factor to interpret the retreat of trench and fragmentation of the subducted paleo-Pacific slab.

Supplementary data to this article can be found online at https://doi.org/10.1016/j.earscirev.2020.103448.

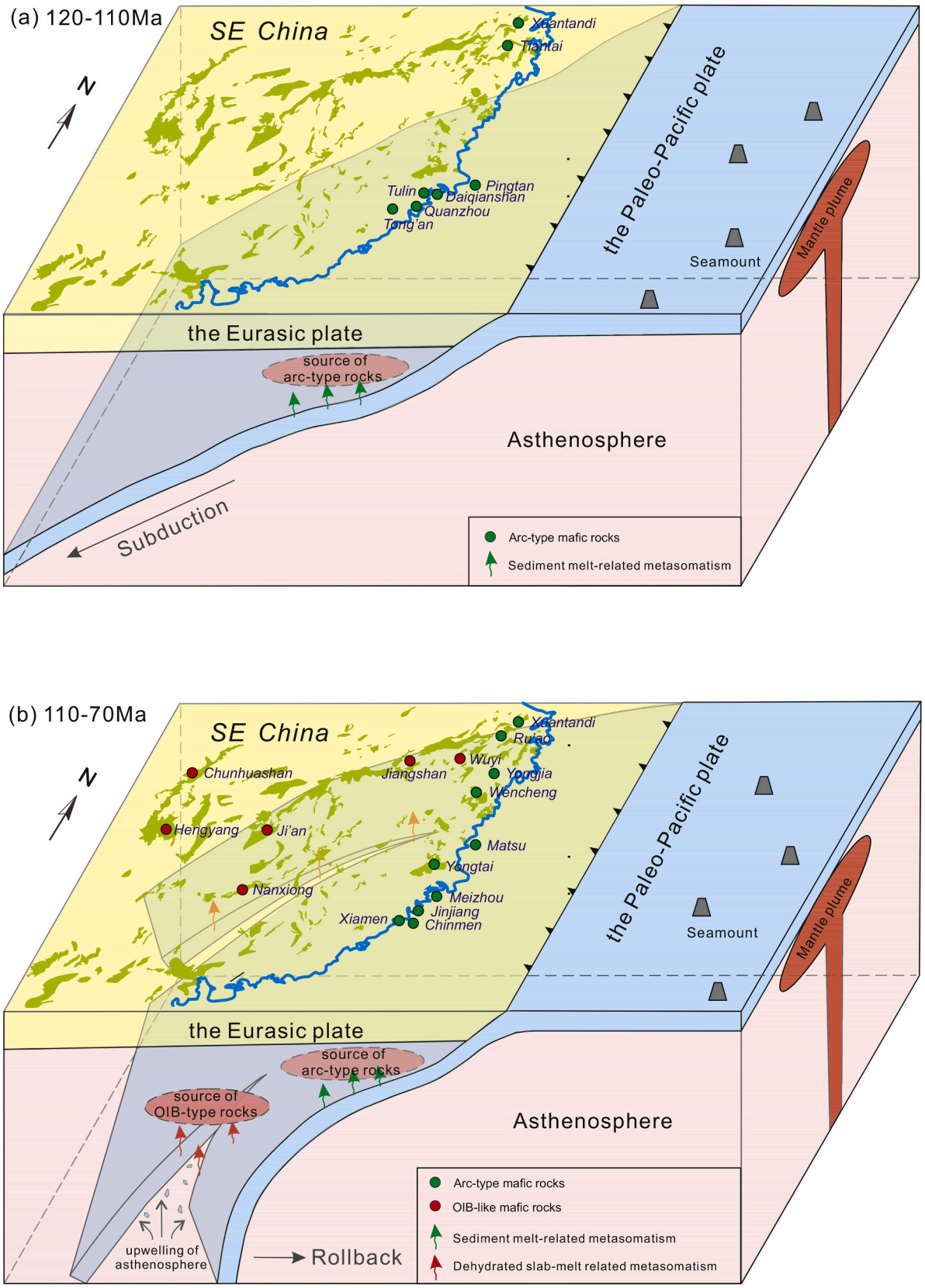

Fig. 16. A tectonic cartoon showing the origin of the Cretaceous mafic magmatism in SE China. (a) Subduction of relatively hot paleo-Pacific Oceanic lithosphere beneath SE China formed the arc-type mafic rocks of 120–110 Ma. (b) During 110–70 Ma, retreat of the trench and rollback of the subducting slab led to breakdown or fragmentation along the subducted oceanic lithosphere, melting of the torn slab occurred to enrich the asthenosphere – the mantle source of OIB-like basalts. See details in the text.

Declaration of Competing Interest

None.

Acknowledgements

We appreciate the helpful and valuable discussions with Profs. Zhongyuan Ren, Weiming Fan, Yuejun Wang, Xuan-Ce Wang, Taiping Zhao during the preparation of the paper. Thanks are due to three anonymous referees and the guest Editor – Prof. Sanzhong Li for their valuable reviews, comments and suggestions, which help greatly improve the manuscript. Prof. Arturo Gómez-Tuena is also thanked for handling. This work was supported by the National Science Foundation of China (Grant Nos. 41525006 and U1701641), the Strategic Priority Research Program (B) of Chinese Academy of Sciences (Grant XDB 18000000), and the Department of Science and Technology of Guangdong Province (2015TX01Z219).

References

Alzawa, Y., Tatsumi, Y., Yamada, H., 1999. Element transport by dehydration of subducted sediments: Implication for arc and ocean island magmatism. Island Arc 8, 38–46.
Ali, S., Ntaflos, T., Upton, B.G.J., 2013. Petrogenesis and mantle source characteristics of Quaternary alkaline mafic lavas in the western Carpathian-Pannonian Region, Styria, Austria. Chem. Geol. 337–338, 99–113.
Bayrakci, G., Minshull, T.A., Sawyer, D.S., Reston, T.J., Klaeschen, D., Papenberg, C., Ranero, C., Bull, J.M., Davy, R.G., Shillington, D.J., Perez-Gussinye, M., Morgan, J. K., 2016. Fault-controlled hydration of the upper mantle during continental rifting. Nat. Geosci. 9, 384–388.
Bédard, J.H., 1994. A procedure for calculating the equilibrium distribution of trace elements among the minerals of cumulate rocks, and the concentration of trace elements in the coexisting liquids. Chem. Geol. 118, 143–153.
Behn, M.D., Kelemen, P.B., Hirth, G., Hacker, B.R., Massonne, H.J., 2011. Diapirs as the source of the sediment signature in arc lavas. Nat. Geosci. 4, 641–646.
Burchfiel, B.C., Royden, L.H., Papanikolaou, D., Pearce, F.D., 2018. Crustal development within a retreating subduction system: the Hellenides. Geosphere 14, 1119–1130.
Burg, J.P., Gerya, T.V., 2005. The role of viscous heating in Barrovian metamorphism of collisional orogens: thermomechanical models and application to the Lepontine Dome in the Central Alps. J. Metamorph. Geol. 23, 75–95.
Castillo, P.R., 2008. Origin of the adakite-high-Nb basalt association and its implications for postsubduction magmatism in Baja California, Mexico. Geol. Soc. Am. Bull. 120, 451–462.
Castro, A., Gerya, T., García-Casco, A., Fernández, C., Díaz-Alvarado, J., Moreno-Ventas, I., Löw, I., 2010. Melting relations of MORB-sediment mélanges in underplated mantle wedge plumes; Implications for the origin of Cordilleran-type batholiths. J. Petrol. 51, 1267–1295.
Chen, J.F., Jahn, B.M., 1998. Crustal evolution of southeastern China: Nd and Sr isotopic evidence. Tectonophysics 284, 101–133.
Chen, C.H., Lin, W.Y., Lu, H.Y., Lee, C.Y., Tien, J.L., Lai, Y.H., 2000. Cretaceous fractionated I-type granitoids and metaluminous A-type granites in SE China: the Late Yanshanian post-orogenic magmatism. Trans. Royal Soc. Edinb. 91, 195–205.
Chen, W.F., Chen, P.R., Xu, X.S., Zhang, M., 2005. Geochemical characteristics of Cretaceous basaltic rocks in South China and constraints on Pacific plate subduction. Sci. China (Ser. D - Earth Sci.) 48, 2104–2117.
Chen, C.H., Lee, C.Y., Shinjo, R., 2008. Was there Jurassic paleo-Pacific subduction in South China?: Constraints from $^{40}Ar/^{39}Ar$ dating, elemental and Sr-Nd-Pb isotopic geochemistry of the Mesozoic basalts. Lithos 106, 83–92.
Chen, Y., Li, W., Yuan, X.H., Badal, J., Teng, J.W., 2015a. Tearing of the Indian lithospheric slab beneath southern Tibet revealed by SKS-wave splitting measurements. Earth Planet. Sci. Lett. 413, 13–24.
Chen, M., Niu, F., Liu, Q., Tromp, J., Zheng, X., 2015b. Multiparameter adjoint tomography of the crust and upper mantle beneath East Asia: 1. Model construction and comparisons. J. Geophys. Res. Solid Earth 120, 1762–1786.
Churikova, T., Dorendorf, F., Wörner, G., 2001. Sources and fluids in the mantle wedge below Kamchatka, evidence from across-arc geochemical variation. J. Petrol. 42, 1567–1593.
Clift, P.D., Vannucchi, P., Morgan, J.P., 2009. Crustal redistribution, crust–mantle recycling and Phanerozoic evolution of the continental crust. Earth-Sci. Rev. 97, 80–104.
Codillo, E.A., Le Roux, V., Marschall, H.R., 2018. Arc-like magmas generated by mélange-peridotite interaction in the mantle wedge. Nature Comm 9, 2864.
Cui, Y.R., Xie, Z., Wang, B., Chen, J.F., Yu, Y.W., He, J.F., 2011. Geochemical characteristics of the Late Mesozoic basalts in southeastern Zhejiang Province and constraints on magma source materials. Geol. J. China Univ. 17, 492–512 (in Chinese with English abstract).
Dai, H.K., Zheng, J.P., O'Reilly, S.Y., Griffin, W.L., Xiong, Q., Xu, R., Su, Y.P., Ping, X.Q., Chen, F.K., 2019. Langshan basalts record recycled Paleo-Asian oceanic materials beneath the northwest North China Craton. Chem. Geol. 524, 88–103.
Dai, L.M., Wang, L.L., Lou, D., Li, Z.H., Dong, H., Ma, F.F., Li, F.K., Li, S.Z., Yu, S.Y., 2020. Slab rollback versus delamination: contrasting fates of flat-slab subduction and implications for South China evolution in the Mesozoic. J. Geophys. Res. Solid Earth 125 (e2019JB019164).
Defant, M.J., Drummond, M.S., 1990. Derivation of some modern arc magmas by melting of young subducted lithosphere. Nature 347, 662–665.
Dong, C.W., Zhou, X.M., Li, H.M., Ren, S.L., Zhou, X.H., 1997. Late Mesozoic crust mantle interaction in Southeastern Fujian: Isotopic evidence from Pingtan igneous complex. Chin. Sci. Bull. 42, 495–498.
Dong, C., Xu, X., Yan, Q., Lin, X., Zhu, G., 2007. A new case of Late Mesozoic crust-mantle interaction in eastern Zhejiang: Geochronology and geochemistry of the Ru'ao diabase-granite composite intrusions. Acta Petrol. Sin. 23, 1303–1312 (in Chinese with English abstract).
Errázuriz-Henao, C., Gómez-Tuena, A., Duque-Trujillo, J., Weber, M., 2019. The role of subducted sediments in the formation of intermediate mantle-derived magmas from the Northern Colombian Andes. Lithos 336, 151–168.
Espinoza, F., Morata, D., Pelleter, E., Maury, R.C., Suárez, M., Lagabrielle, Y., Polvé, M., Bellon, H., Cotten, J., De la Cruz, R., Guivel, C., 2005. Petrogenesis of the Eocene and Mio-Pliocene alkaline basaltic magmatism in Meseta Chile Chico, southern Patagonia, Chile: evidence for the participation of two slab windows. Lithos 82, 315–343.
Fantle, M.S., Tipper, E.T., 2014. Calcium isotopes in the global biogeochemical Ca cycle: implications for development of a Ca isotope proxy. Earth Sci. Rev. 129, 148–177.
Ferrari, L., 2004. Slab detachment control on mafic volcanic pulse and mantle heterogeneity in Central Mexico. Geology 32, 77–80.
Ferrari, L., Petrone, C.M., Francalanci, L., 2001. Generation of oceanic-island basalt-type volcanism in the western Trans-Mexican volcanic belt by slab rollback, asthenosphere infiltration, and variable flux melting. Geology 29, 507–510.
Foley, S., 1992. Vein-plus-wall-rock melting mechanisms in the lithosphere and the origin of potassic alkaline magmas. Lithos 28, 435–453.
Furumura, T., Kennett, B.L.N., 2005. Subduction zone guided waves and the heterogeneity structure of the subducted plate: Intensity anomalies in northern Japan. J. Geophys. Res. Solid Earth 110, 1–27.
Furukawa, Y., Tatsumi, Y., 1999. Melting of a subducting slab and production of high-Mg andesite magmas: Unusual magmatism in SW Japan at 13~15Ma. Geophys Res. Lett. 26, 2271–2274.
Gao, S., Yang, J., Zhou, L., Li, M., Hu, Z., Guo, J., Yuan, H., Gong, H., Xiao, G., Wei, J., 2011. Age and growth of the Archean Kongling terrain, South China, with emphasis on 3.3 Ga granitoid gneisses. Am. J. Sci. 311, 153–182.
Gazel, E., Hoernle, K., Carr, M.J., Herzberg, C., Saginor, I., Van den Bogaard, P., Hauff, F., Feigenson, M., Swisher, C., 2011. Plume-subduction interaction in southern Central America: Mantle upwelling and slab melting. Lithos 121, 117–134.
Gerya, T.V., Yuen, D.A., 2003a. Rayleigh-Taylor instabilities from hydration and melting propel 'cold plumes' at subduction zones. Earth Planet. Sci. Lett. 212, 47–62.
Gerya, T.V., Yuen, D.A., 2003b. Characteristics-based marker-in-cell method with conservative finite-differences schemes for modeling geological flows with strongly variable transport properties. Phys. Earth Planet. Inter. 140, 293–318.
Gerya, T.V., Yuen, D.A., Maresch, W.V., 2004. Thermomechanical modelling of slab detachment. Earth Planet. Sci. Lett. 226, 101–116.
Gómez-Tuena, A., Mori, L., Straub, S.M., 2018a. Geochemical and petrological insights into the tectonic origin of the Transmexican Volcanic Belt. Earth-Sci. Rev. 183, 153–181.
Gómez-Tuena, A., Cavazos-Tovar, J.G., Parolari, M., Straub, S.M., Espinasa-Pereña, R., 2018b. Geochronological and geochemical evidence of continental crust 'relamination' in the origin of intermediate arc magmas. Lithos 322, 52–66.
Gorring, M., Singer, B., Gowers, J., Kay, S.M., 2003. Plio–Pleistocene basalts from the Meseta del Lago Buenos Aires, Argentina: evidence for asthenosphere–lithosphere interactions during slab window magmatism. Chem. Geol. 193, 215–235.
Gréaux, S., Irifune, T., Higo, Y., Tange, Y., Arimoto, T., Liu, Z., Yamada, A., 2019. Sound velocity of $CaSiO_3$ perovskite suggests the presence of basaltic crust in the Earth's lower mantle. Nature 565, 218–221.
Griffin, W.L., Wang, X., Jackson, S.E., Pearson, N.J., O'Reilly, S.Y., 2002. Zircon geochemistry and magma mixing, SE China: in-situ analysis of Hf isotopes, Tonglu and Pingtan igneous complexes. Lithos 61, 237–269.
Grove, T.L., Kinzler, R.J., 1986. Petrogenesis of andesites. Annu. Rev. Earth Planet. Sci. Lett. 14, 417–454.
Guo, F., Nakamura, E., Fan, W.M., Kobayoshi, K., Li, C.W., 2007. Generation of Palaeocene adakitic andesites by magma mixing; Yanji Area, NE China. J. Petrol. 48, 661–692.
Guo, F., Fan, W.M., Li, C.W., Zhao, L., Li, H.X., Yang, J.H., 2012. Multi-stage crust-mantle interaction in SE China: Temporal, thermal and compositional constraints from the Mesozoic felsic volcanic rocks in eastern Guangdong-Fujian provinces. Lithos 150, 62–84.
Guo, F., Li, H.X., Fan, W.M., Li, J.Y., Zhao, L., Huang, M.W., Xu, W.L., 2015. Early Jurassic subduction of the Paleo-Pacific Ocean in NE China: Petrologic and geochemical evidence from the Tumen mafic intrusive complex. Lithos 224–225, 46–60.
Guo, F., Li, H.X., Fan, W.M., Li, J.Y., Zhao, L., Huang, M.W., 2016. Variable sediment flux in generation of Permian subduction-related mafic intrusions from the Yanbian region, NE China. Lithos 261, 195–215.
Hale, A.J., Gottschaldt, K.D., Rosenbaum, G., Bourgouin, L., Bauchy, M., Mühlhaus, H., 2010. Dynamics of slab tear faults: Insights from numerical modelling. Tectonophysics 483, 58–70.
Hanyu, T., Tatsumi, Y., Nakai, S., Chang, Q., Miyazaki, T., Sato, K., Tani, K., Shibata, T., Yoshida, T., 2006. Contribution of slab melting and slab dehydration to magmatism

in the NE Japan arc for the last 25 Myr: constraints from geochemistry. Geophys. Geochem. Geosyst. 7, Q08002.
Hastie, A.R., Mitchell, S.F., Kerr, A.C., Minifie, M.J., Millar, I.L., 2011. Geochemistry of rare high-Nb basalt lavas: are they derived from a mantle wedge metasomatised by slab melts? Geochim. Cosmochim. Acta 75, 5049–5072.
Hauff, F., Hoernle, K., Schmidt, A., 2003. Sr-Nd-Pb composition of Mesozoic Pacific oceanic crust (Site 1149 and 801, ODP Leg 185): Implications for alteration of ocean crust and the input into the Izu-Bonin-Mariana subduction system. Geochem. Geophys. Geosyst. 4, 8913. https://doi.org/10.1029/2002GC000421.
Hermann, J., Spandler, C.J., 2008. Sediment melts at sub-arc depths: an experimental study. J. Petrol. 49, 717–740.
Herrstrom, E.A., Reagan, M.K., Morris, J.D., 1995. Variations in lava composition associated with flow of asthenosphere beneath southern Central America. Geology 23, 617–620.
Herzberg, C., 2011. Identification of source lithology in the Hawaiian and Canary Islands: implications for origins. J. Petrol. 52, 113–146.
Hirschmann, M.M., Kogiso, T., Baker, M.B., Stolper, E.M., 2003. Alkalic magmas generated by partial melting of garnet pyroxenite. Geology 31, 481–484.
Hoernle, K., White, J.D.L., van den Bogaard, P., Hauff, F., Coombs, D.S., Werner, R., Timm, C., Garbe-Schonberg, D., Reay, A., Cooper, A.F., 2006. Cenozoic intraplate volcanism on New Zealand: Upwelling induced by lithospheric removal. Earth Planet. Sci. Lett. 248, 350–367.
Hoffman, A.W., 1997. Mantle geochemistry: the messages from oceanic volcanism. Nature 385, 219–229.
von Huene, R., Scholl, D.W., 1991. Observations at convergent margins concerning sediment subduction, subduction erosion, and the growth of continental crust. Rev. Geophys. 29, 279–316.
Ishikawa, A., Kuritani, T., Makishima, A., Nakamura, E., 2007. Ancient recycled crust beneath the Ontong Java Plateau: isotopic evidence from the garnet clinopyroxenite xenoliths, Malaita. Solomon Islands. Earth Planet. Sci. Lett. 259, 134–148.
Ishizaka, K., Carlson, R.W., 1983. Nd-Sr systematics of the Setouchi volcanic rocks, South-west Japan: a clue to the origin of orogenic andesite. Earth Planet. Sci. Lett. 64, 327–340.
James, D.E., Fouch, M.J., Carlson, R.W., Roth, J.B., 2011. Slab fragmentation, edge flow and the origin of the Yellowstone hotspot track. Earth Planet. Sci. Lett. 311, 124–135.
Jia, Z.B., Chen, H., Xia, Q.K., Liu, J., Zhu, K.Y., Wang, P.Y., Markhand, A.H., 2020. Influence of the subduction of the Pacific plate on the mantle characteristics of South China: Constraints from the temporal geochemical evolution of the Mesozoic basalts in the Jitai Basin. Lithos 105, 352–353.
Kelemen, P.B., Hanghøj, K., Greene, A.R., 2013. One View of the Geochemistry of Subduction-Related Magmatic Arcs, with an Emphasis on Primitive Andesite and Lower Crust. In: Treatise on Geochemistry, Second edition. Elsevier, pp. 749–806.
Kepezhinskas, P., McDermott, M., Defant, M.J., Hochstaedter, A., Drummond, M.S., Hawkesworth, C.J., Koloskov, A., Maury, R.C., Bellon, H., 1997. Trace element and Sr-Nd-Pb isotopic constraints on a three-component model of Kamchatka Arc petrogenesis. Geochim. Cosmochim. Acta 61, 577–600.
Kincaid, C., Griffiths, R.W., 2003. Laboratory models of the thermal evolution of the mantle during rollback subduction. Nature 425, 58–62.
Klemme, S., Prowatke, S., Hametner, K., Günther, D., 2005. Partitioning of trace elements between rutile and silicate melts: Implications for subduction zones. Geochim. Cosmochim. Acta 69, 2361–2371.
Kogiso, T., Tatsumi, Y., Nakano, S., 1997. Trace element transport during dehydration processes in the subducted oceanic crust. 1. Experiments and implications for the origin of ocean island basalts. Earth Planet. Sci. Lett. 148, 193–205.
Kogiso, T., Hirschmann, M.M., Frost, D.J., 2003. High-pressure partial melting of garnet pyroxenite: possible mafic lithologies in the source of ocean island basalts. Earth Planet. Sci. Lett. 216, 603–617.
La Flèche, M.R., Camiré, G., Jenner, G.A., 1998. Geochemistry of post-Acadian, Carboniferous continental intraplate basalts from the Maritimes Basin, Magdalen Islands, Québec. Canada. Chem. Geol. 148, 115–136.
Labanieh, S., Chauvel, C., Germa, A., Quidelleur, X., Lewin, E., 2010. Isotopic hyperbolas constrain sources and processes under the Lesser Antilles arc. Earth Planet. Sci. Lett. 298, 35–46.
Lambart, S., Laporte, D., Schiano, P., 2009. An experimental study of pyroxenite partial melts at 1 and 1.5GPa: Implications for the major-element composition of Mid-Ocean Ridge Basalts. Earth Planet. Sci. Lett. 288, 335–347.
Lambart, S., Laporte, D., Provost, A., Schiano, P., 2012. Fate of pyroxenite-derived melts in the peridotitic mantle: thermodynamic and experimental constraints. J. Petrol. 53, 451–476.
Lambart, S., Baker, M.B., Stolper, E.M., 2016. The role of pyroxenite in basalt genesis: Melt-PX, a melting parameterization for mantle pyroxenites between 0.9 and 5 GPa. J. Geophys. Res. 121, 5708–5735.
Lapierre, H., Jahn, B.M., Charvet, J., Yu, Y.W., 1997. Mesozoic felsic arc magmatism and continental olivine tholeiites in Zhejiang province and their relationship with the tectonic activity in southeastern China. Tectonophysics 274, 321–338.
Li, X.H., 2000. Cretaceous magmatism and lithospheric extension in Southeast China. J. Asian Earth Sci. 18, 293–305.
Li, Z.X., Li, X.H., 2007. Formation of the 1300-km-wide intracontinental orogen and postorogenic magmatic province in Mesozoic South China: a flat-slab subduction model. Geology 35, 179–182.
Li, C., van der Hilst, R.D., 2010. Structure of the upper mantle and transition zone beneath Southeast Asia from traveltime tomography. J. Geophys. Res. Solid Earth 115, B07308.
Li, X.H., Li, W.X., Li, Z.X., Lo, C.H., Wang, J., Ye, M.F., Yang, Y.H., 2009. Amalgamation between the Yangtze and Cathaysia Blocks in South China: Constraints from SHRIMP U-Pb zircon ages, geochemistry and Nd-Hf isotopes of the Shuangxiwu volcanic rocks. Precambrian Res. 174, 117–128.
Li, J.H., Zhang, Y.Q., Dong, S.W., Johnston, S.T., 2014a. Cretaceous tectonic evolution of South China: a preliminary synthesis. Earth-Sci. Rev. 134, 98–136.
Li, Z., Qiu, J.S., Yang, X.M., 2014b. A review of the geochronology and geochemistry of Late Yanshanian (Cretaceous) plutons along the Fujian coastal area of southeastern China: Implications for magma evolution related to slab break-off and rollback in the Cretaceous. Earth-Sci. Rev. 128, 232–248.
Li, C.S., Arndt, N.T., Tang, Q.Y., Ripley, E.M., 2015. Trace element indiscrimination diagrams. Lithos 232, 76–83.
Li, Z., Wang, X.C., Wilde, S.A., Liu, L., Li, W.X., Yang, X., 2018. Role of deep-Earth water cycling in the growth and evolution of continental crust: Constraints from Cretaceous magmatism in Southeast China. Lithos 302–303, 126–141.
Li, S.Z., Suo, Y.H., Li, X.Y., Zhou, J., Santosh, M., Wang, P.C., Wang, G.Z., Guo, L.L., Yu, S.Y., Lan, H.Y., Dai, L.M., Zhou, Z.Z., Cao, X.Z., Zhu, J.J., Liu, B., Jiang, S.H., Wang, G., Zhang, G.W., 2019. Mesozoic tectono-magmatic response in the East Asian ocean-continent connection zone to subduction of the Paleo-Pacific Plate. Earth-Sci. Rev. 192, 91–137.
Liao, Q.A., Wang, J.M., Xue, C.S., Li, C.N., 1999. The characteristics of two kinds basalts in cretaceous basin and their relations with the basin's evolution, in Shangrao-Guangfeng district, Jiangxi province. Acta Petrol. Sin. 15, 116–123.
Liao, J., Gerya, T., Thielmann, M., Webb, A.G., Kufner, S.K., Yin, A., 2017. 3D geodynamic models for the development of opposing continental subduction zones: the Hindu Kush–Pamir example. Earth Planet. Sci. Lett. 480, 133–146.
Liao, J., Maluà, M.G., Zhao, L., Baldwin, S.L., Fitzgerald, P.G., Gerya, T., 2018. Divergent plate motion drives rapid exhumation of (ultra) high pressure rocks. Earth Planet. Sci. Lett. 491, 67–80.
Liu, L., Xu, X.S., Zou, H.B., 2012. Episodic eruptions of the late Mesozoic volcanic sequences in southeastern Zhejiang, SE China: Petrogenesis and implications for the geodynamics of paleo-Pacific subduction. Lithos 154, 166–180.
Liu, S.C., Xia, Q.K., Choi, S.H., Deloule, E., Li, P., Liu, J., 2016a. Continuous supply of recycled Pacific oceanic materials in the source of Cenozoic basalts in SE China: the Zhejiang case. Contrib. Mineral. Petrol. 171, 1–31.
Liu, L., Xu, X., Xia, Y., 2016b. Asynchronizing paleo-Pacific slab rollback beneath SE China: Insights from the episodic late Mesozoic volcanism. Gondwana Res. 37, 397–407.
Márquez, A., Oyarzun, R., Doblas, M., Verma, S.P., 1999. Alkalic (ocean-island basalt type) and calc-alkalic volcanism in the Mexican volcanic belt: a case for plume-related magmatism and propagating rifting at an active margin? Geology 27, 51–54.
Marschall, H.R., Schumacher, J.C., 2012. Arc magmas sourced from mélange diapirs in subduction zones. Nat. Geosci. 5, 862–867.
Martin, H., Smithies, R.H., Rapp, R., Moyen, J.F., Champion, D., 2005. An overview of adakite, tonalite–trondhjemite–granodiorite (TTG), and sanukitoid: relationships and some implications for crustal evolution. Lithos 79, 1–24.
Maruyama, S., Isozaki, Y., Kimura, G., Terabayashi, M., 1997. Paleogeographic maps of the Japanese Islands: Plate tectonic synthesis from 750 Ma to the present. Island Arc 6, 121–142.
Meng, L.F., Li, Z.X., Chen, H., Li, X.H., Wang, X.C., 2012. Geochronological and geochemical results from Mesozoic basalts in southern South China Block support the flat-slab subduction model. Lithos 132, 127–140.
Miller, M.S., Gorbatov, A., Kennett, B.L.N., 2005. Heterogeneity within the subducting Pacific slab beneath the Izu-Bonin-Mariana arc: evidence from tomography using 3D ray tracing inversion techniques. Earth Planet. Sci. Lett. 235, 331–342.
Mullen, E.K., Weis, D., 2013. Sr-Nd-Hf-Pb isotope and trace element evidence for the origin of alkalic basalts in the Garibaldi Belt, northern Cascade arc. Geochem. Geophys. Geosyst. 14, 3126–3155.
Müller, R.D., Seton, M., Zahirovic, S., Williams, S.E., Matthews, K.J., Wright, N.M., Shephard, G.E., Maloney, K.T., Barnett-Moore, N., Hosseinpour, M., Bower, D.J., Cannon, J., 2016. Ocean basin evolution and global-scale plate reorganization events since pangea breakup. Annu. Rev. Earth Planet. Sci. 44, 107–138.
Nakakuki, T., Mura, E., 2013. Dynamics of slab rollback and induced back-arc basin formation. Earth Planet. Sci. Lett. 361, 287–297.
Nebel, O., Vroon, P.Z., van Westrenen, W., Iizuka, T., Davies, G.R., 2011. The effect of sediment recycling in subduction zones on the Hf isotope character of new arc crust, Banda arc. Indonesia. Earth Planet. Sci. Lett. 303, 240–250.
Nichols, G.T., Wyllie, P.J., Stern, C.R., 1994. Subduction zone melting of pelagic sediments constrained by melting experiments. Nature 371, 785–788.
Nielsen, S.G., Marschall, H.R., 2017. Geochemical evidence for mélange melting in global arcs. Sci. Adv. 3, 1–7.
Parolari, M., Gómez-Tuena, A., Cavazos-Tovar, J.G., Hernández-Quevedo, G., 2018. A balancing act of crust creation and destruction along the western Mexican convergent margin. Geology 46, 455–458.
Peacock, S.M., Rushmer, T., Thompson, A.B., 1994. Partial melting of subducting oceanic-crust. Earth Planet. Sci. Lett. 212, 227–244.
Plank, T., 2014. The chemical composition of subducting sediments. In: Holland, H.D., Turekian, K.K. (Eds.), Treatise on Geochemistry, Second edition. Elsevier Ltd., Amsterdam, pp. 607–629.
Plank, T., Langmuir, C., 1998. The chemical composition of subducting sediment and its consequences for the crust and mantle. Chem. Geol. 145, 325–394.
Plank, T., Kelley, K.A., Zimmer, M.M., Hauri, E.H., Wallace, P.J., 2013. Why do mafic arc magmas contain ~4wt% water on average? Earth Planet Sci. Lett. 364, 168–179.
Prelević, D., Akal, C., Romer, R.L., Mertz-Kraus, R., Helvacı, C., 2015. Magmatic response to slab tearing: constraints from the afyon alkaline volcanic complex, Western Turkey. J. Petrol. 56, 527–562.

Qin, S.C., Fan, W.M., Guo, F., Li, C.W., Gao, X.F., 2010. Petrogenesis of late mesozoic diabase dikes in zhejiang-fujian provinces: constraints from Ar-Ar dating and geochemistry. Acta Petrol. Sin. 26, 3295–3306 (in Chinese with English abstract).
Qin, S.C., Fan, W.M., Guo, F., 2019. Petrogenesis and geodynamic implications of late Mesozoic mafic volcanic rocks along the Jiangshan-Shaoxing fault in SE China. Acta Petrol. Sin. 35, 1892–1906 (In Chinese with English abstract).
Reagan, M.K., Gill, J.B., 1989. Coexisting calcalkaline and high-niobium basalts from Turrialba Volcano, Costa Rica: Implications for residual titanates in arc magma sources. J. Geophys. Res. 94, 4619–4633.
Ren, Z.Y., Ingle, S., Takahashi, E., Hirano, N., Hirata, T., 2005. The chemical structure of the Hawaiian mantle plume. Nature 436, 837–840.
Rosenbaum, G., Agostinetti, N.P., 2015. Crustal and upper mantle responses to lithospheric segmentation in the northern Apennines. Tectonics 34, 648–661.
Rosenbaum, G., Gasparon, M., Lucente, F.P., Peccerillo, A., Miller, M.S., 2008. Kinematics of slab tear faults during subduction segmentation and implications for Italian magmatism. Tectonics 27 (2).
Rudnick, R.L., Gao, S., 2014. Composition of the continental crust. In: Holland, H.D., Turekian, K.K. (Eds.), Treatise on Geochemistry, Second edition. Elsevier Ltd., Amsterdam, pp. 1–51.
Scholl, D.W., Von Huene, R., 2010. Subduction zone recycling processes and the rock record of crustal suture zone. Can. J. Earth Sci. 47, 633–654.
Seton, M., Muller, R.D., Zahirovic, S., Gaina, C., Torsvik, T.H., Shephard, G., Talsma, A., Gurnis, M., Turner, M., Maus, S., Chandler, M., 2012. Global continental and ocean basin reconstructions since 200 Ma. Earth-Sci. Rev. 113, 212–270.
Shimoda, G., Tatsumi, Y., Nohda, S., Ishizaka, K., Jahn, B.M., 1998. Setouchi high-Mg andesites revisited: Geochemical evidence for melting of subducting sediments. Earth Planet. Sci. Lett. 160, 479–492.
Shu, L.S., Deng, P., Wang, B., Tan, Z.Z., Yu, X.Q., Sun, Y., 2004. Lithology, kinematics and geochronology related to late Mesozoic basin-mountain evolution in the Nanxiong-Zhuguang area. South China. Sci. China Ser. Earth Sci. 47, 673–688.
Sobolev, A.V., Hofmann, A.W., Kuzmin, D.V., Yaxley, G.M., Arndt, N.T., Chung, S.L., Danyushevsky, L.V., Elliott, T., Frey, F.A., Garcia, M.O., et al., 2007. The amount of recycled crust in sources of mantle-derived melts. Science 316, 412–417.
Spandler, C., Pirard, C., 2013. Element recycling from subducting slabs to arc crust: a review. Lithos 170–171, 208–223.
Stern, R.J., 2002. Subduction zones. Rev. Geophys. 40, 1012–1053.
Stern, R.J., 2004. Subduction initiation: spontaneous and induced. Earth Planet Sci Lett. 226, 275–292.
Stolz, A.J., Jochum, K.P., Spettel, B., Hofmann, A.W., 1996. Fluid- and melt-related enrichment in the subarc mantle: evidence from Nb/Ta variations in island-arc basalts. Geology 24, 443–446.
Stracke, A., Bizimis, M., Salters, V.J.M., 2003. Recycling oceanic crust: Quantitative constraints. Geochem. Geophys. Geosyst. 4, 8003.
Straub, S.M., Gomez-Tuena, A., Stuart, F.M., Zellmer, G.F., Espinasa-Perena, R., Cai, Y., Iizuka, Y., 2011. Formation of hybrid arc andesites beneath thick continental crust. Earth Planet. Sci. Lett. 303, 337–347.
Sun, S.S., McDonough, W.F., 1989. Chemical and isotopic systematics of oceanic basalts: Implications for mantle composition and processes. Geol. Soc. Lond. Spec. Pub. 42, 313–345.
Sun, W.D., Ding, X., Hu, Y.H., Li, X.H., 2007. The golden transformation of the cretaceous plate subduction in the West Pacific. Earth Planet. Sci. Lett. 262, 533–542.
Suo, Y.H., Li, S.Z., Jin, C., Zhang, Y., Zhou, J., Li, X.Y., Wang, P.C., Liu, Z., Wang, X.Y., Somerville, I., 2019. Eastward tectonic migration and transition of the Jurassic-cretaceous Andean-type continental margin along Southeast China. Earth-Sci. Rev. 196, 102884.
Syracuse, E.M., van Keken, P.E., Abers, G.A., 2010. The global range of subduction zone thermal models. Phys. Earth Planet. Inter. 183, 73–90.
Tatsumi, Y., Shukuno, H., Sato, K., Shibata, T., Yoshikawa, M., 2003. The petrology and geo-chemistry of high-magnesium andesites at the Western tip of the Setouchi volcanic belt, SW Japan. J. Petrol. 44, 1561–1578.
Tejada, M.L.G., Mahoney, J.J., Duncan, R.A., Hawkins, M.P., 1996. Age and geochemistry of basement and alkalic rocks of Malaita and Santa Isabel, Solomon Islands, Southern Margin of Ontong Java Plateau. J. Petrol. 37, 361–394.
Vervoort, J.D., Blichert-Toft, J., Patchett, P.J., Albarede, F., 1999. Relationships between Lu-Hf and Sm-Nd isotopic systems in the global sedimentary system. Earth Planet. Sci. Lett. 168, 79–99.
Wang, Y.J., Fan, W.M., Guo, F., Peng, T.P., Li, C.W., 2003. Geochemistry of Mesozoic mafic rocks adjacent to the Chenzhou-Linwu fault, South China: Implications for the lithospheric boundary between the Yangtze and Cathaysia blocks. Inter. Geol. Rev. 45, 263–286.
Wang, Y., Fan, W., Cawood, P.A., Li, S., 2008. Sr-Nd-Pb isotopic constraints on multiple mantle domains for Mesozoic mafic rocks beneath the South China Block hinterland. Lithos 106, 297–308.
Wang, X.C., Li, Z.X., Li, X.H., Li, J., Liu, Y., Long, W.G., Zhou, J.B., Wang, F., 2012. Temperature, pressure, and composition of the mantle source region of late Cenozoic basalts in Hainan island, SE Asia: a consequence of a young thermal mantle plume close to subduction zones? J. Petrol. 53, 177–233.
Wang, Y.J., Fan, W.M., Zhang, G.W., Zhang, Y.H., 2013. Phanerozoic tectonics of the South China Block: Key observations and controversies. Gondwana Res. 23, 1273–1305.
Wang, G.G., Ni, P., Zhao, C., Wang, X.L., Li, P.F., Chen, H., Zhu, A.D., Li, L., 2016. Spatiotemporal reconstruction of late Mesozoic silicic large igneous province and related epithermal mineralization in South China: Insights from the Zhilingtou volcanic-intrusive complex. J. Geophys. Res. Solid Earth 121, 7903–7928.
Watt, S.F.L., Pyle, D.M., Mather, T.A., Naranjo, J.A., 2013. Arc magma compositions controlled by linked thermal and chemical gradients above the subducting slab. Geophys. Res. Lett. 40, 2550–2556.
Weaver, B.L., 1991. The origin of ocean island basalt end-member compositions: Trace element and isotopic constraints. Earth Planet. Sci. Lett. 104, 381–397.
White, W.M., 2015. Isotope Geochemistry. John Wiley & Sons Inc, New York, pp. 1–496.
White, W.M., Dupré, B., 1986. Sediment subduction and magma genesis in the Lesser Antilles: Isotopic and trace element constraints. J. Geophys. Res. 91, 5927.
Wilson, M., 1989. Igneous Petrogenesis. Springer, Harper Collins Academic, London.
Woodhead, J.D., Hergt, J.M., Davidson, J.P., Eggins, S.M., 2001. Hafnium isotope evidence for 'conservative' element mobility during subduction zone processes. Earth Planet. Sci. Lett. 192 (3), 331–346.
Workman, R.K., Hart, S.R., 2005. Major and trace element composition of the depleted MORB mantle (DMM). Earth Planet. Sci. Lett. 231, 53–72.
Wu, Y., Guo, F., Wang, X.C., Zhang, B., Zhang, X., Alemayehu, M., Wang, G., 2020. Generation of late cretaceous Ji'an basalts through asthenosphere-slab interaction in South China. Geol. Soc. Am. Bull. 132, 1316–1332.
Xie, X., Xu, X.S., Zou, H.B., Xing, G.F., 2001. Trace element and Nd-Sr-Pb isotope studies of Mesozoic and Cenozoic basalts in coastal area of SE China. Acta Petrol. Sin. 17, 617–628 (in Chinese with English abstract).
Xie, G.Q., Hu, R.Z., Mao, J.W., Pirajno, F., Li, R.L., Cao, J.J., Jiang, G.H., Zhao, J.H., 2006. K-Ar dating, geochemical, and Sr-Nd-Pb isotopic systematics of late Mesozoic mafic dikes, southern Jiangxi Province, Southeast China: Petrogenesis and tectonic implications. Inter. Geol. Rev. 48, 1023–1051.
Xu, X.S., Dong, C.W., Li, W.X., Zhou, X.M., 1999. Late Mesozoic intrusive complexes in the coastal area of Fujian, SE China: the significance of the gabbro-diorite-granite association. Lithos 46, 299–315.
Yang, Z.L., Shen, W.Z., Tao, K.Y., Shen, J.L., 1999. Sr, Nd and Pb isotopic characteristics of early cretaceous basaltic rocks from the coast of Zhejiang and Fujian:Evidences for ancient enriched mantle source. Chin. J. Geol. 34, 59–68 (in Chinese with English abstract).
Yu, X.Q., Shu, L.S., Yan, T.Z., Yu, Y.W., Zu, F.P., Wang, B., 2004. Geochemistry of basalts of late period of early cretaceous from Jiangshan-Guangfeng, SE China and its tectonic significance. Geochimica 33, 465–476 (in Chinese with English abstract).
Yu, J., O'Reilly, Y.S., Wang, L., Griffin, W.L., Jiang, S., Wang, R., Xu, X., 2007. Finding of ancient materials in Cathaysia and implication for the formation of Precambrian crust. Chin. Sci. Bull. 52, 13–22.
Zanetti, A., Mazzucchelli, M., Rivalenti, G., Vannucci, R., 1999. The Fineo phlogopite-peridotite massif: an example of subduction-related metasomatism. Contrib. Mineral. Petrol. 134, 107–122.
Zeng, G., Chen, L.H., Hofmann, A.W., Jiang, S.Y., Xu, X.S., 2011. Crust recycling in the sources of two parallel volcanic chains in Shandong. North China. Earth Planet. Sci. Lett. 302, 359–368.
Zeng, G., He, Z.Y., Li, Z., Xu, X.S., Chen, L.H., 2016. Geodynamics of paleo-Pacific plate subduction constrained by the source lithologies of late Mesozoic basalts in southeastern China. Geophys. Res. Lett. 43, 10,189–10,197.
Zhang, B., Guo, F., Zhang, X.B., Wu, Y.M., Wang, G.Q., Zhao, L., 2019. Early cretaceous subduction of Paleo-Pacific Ocean in the coastal region of SE China: Petrological and geochemical constraints from the mafic intrusions. Lithos 334, 8–24.
Zhang, B., Guo, F., Zhang, X., Wu, Y., Wang, G., Zhao, L., 2020. Origin of the early cretaceous Liucheng OIB-type dolerite sill in Zhejiang Province, coastal region of SE China: Implications for recycling of the Paleo-Pacific slab. J. Asian Earth Sci. 193, 104330.
Zhao, J.H., Hu, R., Zhou, M.F., Liu, S., 2007. Elemental and Sr-Nd-Pb isotopic geochemistry of Mesozoic mafic intrusions in southern Fujian Province, SE China: Implications for lithospheric mantle evolution. Geol. Mag. 144, 937–952.
Zhao, L., Guo, F., Fan, W.M., Zhang, Q.W., Wu, Y.M., Li, J.Y., Yan, W., 2016. Early cretaceous potassic volcanic rocks in the Jiangnan Orogenic Belt, East China: Crustal melting in response to subduction of the Pacific-Izanagi ridge. Chem. Geol. 437, 30–43.
Zhao, L., Guo, F., Fan, W., Huang, M., 2019. Roles of subducted pelagic and terrigenous sediments in early Jurassic mafic magmatism in NE China: Constraints on the architecture of Paleo-Pacific subduction zone. J. Geophys. Res. Solid Earth 124, 2525–2550.
Zhou, X.M., Li, W.X., 2000. Origin of late Mesozoic igneous rocks in Southeastern China: implications for lithosphere subduction and underplating of mafic magmas. Tectonophysics 326, 269–2877.
Zhou, X.M., Sun, T., Shen, W.Z., Shu, L.S., Niu, Y.L., 2006. Petrogenesis of Mesozoic granitoids and volcanic rocks in South China: a response to tectonic evolution. Episodes 29, 26–33.
Zou, H.B., Zindler, A., Xu, X.S., Qi, Q., 2000. Major, trace element, and Nd, Sr and Pb isotope studies of Cenozoic basalts in SE China: mantle sources, regional variations, and tectonic significance. Chem. Geol. 171, 33–47.